Ancient TL

Single-aliquot Regenerative-Dose (SAR) and Standardised Growth Curve (SGC) Equivalent Dose Determination in a Batch Model Using the R Package 'numOSL'

Jun Peng[1] and Bo Li[2*]

[1]School of Resource Environment and Safety Engineering,
Hunan University of Science and Technology, Xiangtan 411201, China
[2]Centre for Archaeological Science, School of Earth and Environmental Sciences,
University of Wollongong, Wollongong, NSW 2522, Australia

*Corresponding Author: bli@uow.edu.au

Received: November 1, 2017; in final form: December 12, 2017

Abstract

The single-aliquot regenerative-dose (SAR) protocol is widely used for determining equivalent dose (D_e) in optically stimulated luminescence (OSL) dating of Quaternary sediments. The standardised growth curve (SGC) method has been used as an efficient procedure to save measurement time for OSL measurements. The analysis of OSL signals and SAR data to determine D_e estimates and to establish SGC, however, usually involves a large amount of tedious work and is very time consuming, especially when a large number of aliquots or grains are measured and analysed. Here we present transparent and easy-to-use R functions to analyse OSL data sets obtained using SAR procedures in a batch model under the framework of the R package `'numOSL'`. These functions allow users to: (1) import and select data records from single or multiple BIN (or BINX) file; (2) analyse OSL signals and determine their standard errors, based on either a Poisson distribution or a non-Poisson (over-dispersed) distribution in counting statistics; (3) establish dose response curves (DRC) with a range of fitting functions, including a general order kinetic (GOK) function; (4) calculate SAR D_e and associated error using either a Monte Carlo simulation or a simple transformation method; (5) select reliable SAR D_e estimates based on a variety of rejection criteria; (6) select well-behaved DRCs to establish SGC using a least-square normalisation (LS-normalisation) procedure and calculate SGC D_e; (7) graphically summarise and report the results. Worked examples are provided to demonstrate the above functions using experimentally obtained data sets. The relevant R code templates are provided.

Keywords: OSL dating; SAR; SGC; Batch model; R package numOSL

1. Introduction

The single-aliquot regenerative-dose (SAR) protocol (Galbraith et al., 1999; Murray & Wintle, 2000) has been successfully applied to determining equivalent dose (D_e) of sediments from a wide variety of Quaternary environments (Murray & Olley, 2002; Roberts et al., 2015). A standard SAR procedure involves the measurement of natural signals and a series of regenerative-dose signals, together with their corresponding test-dose signals, to establish dose response curves (DRC) using the sensitivity-corrected signals. SAR data analysis usually involves a number of processes, including calculating signal intensities and their associated errors, fitting DRC, determining D_e estimates and their associated errors based on natural signals and DRCs, with application of a number of rejection criteria to select reliable D_e (e.g., Wintle & Murray, 2006; Jacobs et al., 2003, 2006).

SAR D_e analysis is routinely performed using the popular and user-friendly software package *Analyst* (Duller, 2015). In *Analyst*, D_e analysis can be performed interactively by the user with real-time and visual adjustment of parameters and manually choosing analysing methods. For single-grain analysis, *Analyst* provides a simple way for automatically analysing SAR data through the function menu "Analyse All Grains". The interactive process, on the other hands, may be tedious and time-consuming if the user wants to compare

D_e values selected using different rejection criteria settings. Moreover, it is difficult to integrate and graphically report the results of large numbers of aliquots (grains), and only a brief statistical report of data manipulation is provided. There is also an **R** package called `'Luminescence'` (Kreutzer et al., 2012) that provides many functions for SAR D_e calculation. However, only a limited number of rejection criteria are provided to select D_e estimates in this package.

The standardised growth curve (SGC) procedure (Roberts & Duller, 2004) has been proposed to save instrument time for D_e determination, because this method requires solely the measurements of the sensitivity-corrected natural signal (L_n/T_n). This method has been successfully applied to date sedimentary samples from different regions (Burbidge et al., 2006; Lai, 2006; Stevens et al., 2007; Telfer et al., 2008; Long et al., 2010; Yang et al., 2011; Shen & Mauz, 2011). The original SGC method was recently improved by Li et al. (2015a,b), by incorporating an additional regenerative dose for normalising the natural signals from different aliquots (grains), the so-called "re-normalisation" procedure. Based on this new method, it is possible to establish common SGCs not only for samples from the same site but also for samples from different regions. The re-normalisation procedure was subsequently further improved using a more generalised procedure that involves multiple iterative scaling and fitting processes, the so-called "least-squares normalisation" (LS-normalisation) procedure (Li et al., 2016). An increasing number of studies have successfully applied the improved SGC methods (e.g., Guo et al., 2016; Hu et al., 2016; Jacobs et al., 2017; Fu et al., 2017). The process for selecting reliable growth curves and applying the LS-normalisation procedures to establish SGCs and calculate SGC D_e, however, is non-trivial and involves a large amount of data handling.

In this study, we present easy-to-use standardised programmes for analysing, summarising, and reporting single-grain or single-aliquot SAR data in a batch model, and selecting well-behaved DRCs and applying the LS-normalisation procedure to establish SGCs and calculate D_e values. In contrast to manual operation, in batch processing, jobs are queued and processed internally one after the other without manual intervention. It thus provides an easier and more convenient way to analyse and report large SAR data sets. Our functions have already been released under the framework of the **R** package `'numOSL'` (version 2.3) (https://cran.r-project.org/package=numOSL) (Peng et al., 2013). These functions are self-contained and do not depend on any external **R** packages. Codes were programmed using the Fortran 90 programming language and were wrapped by **R** using an interface to improve efficiency and running speed. We presented here detailed implementation of SAR and SGC D_e analysis using simple **R** code templates. The report for these templates was automatically generated using the **R** package `'knitr'` (Xie, 2015) and an example is provided in the supplementary materials.

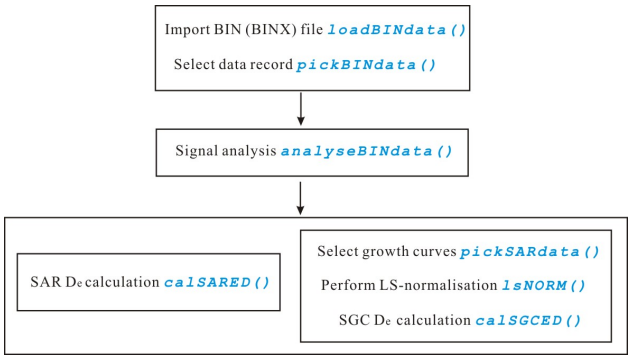

Figure 1. Workflows of SAR and SGC D_e analysis using functions in **R** package `'numOSL'`.

2. D_e analysis using the `'numOSL'` package

SAR and SGC D_e analysis can be separated into three major steps: (1) data import and selection; (2) signal analysis; and (3) D_e calculation and summarising. These steps and relevant functions are described graphically using the workflow shown in Fig. 1, and are elaborated as follows.

2.1. Data import and selection

The function `loadBINdata()` loads standard luminescence data stored in files with extension ".BIN" or ".BINX" into **R**. It can load a single file or multiple files simultaneously. The output of this function is an object of S3 class "loadBIN" containing loaded data records (`$records`) and a summary table (`$tab`). The summary table showing the attributions of each record can be visualized by setting argument `view=TRUE`.

Once the data are loaded, the function `pickBINdata()` can be used to select data records stored in the object "loadBIN" according to various attributions of each signal record, such as position number (`Position`), grain number (`Grain`), run number (`Run`), set number (`Set`), data type (`DType`), irradiation time (`IRRTime`), etc. The selected records are summarised in a table as shown in Fig. 2. The selected records can also be further filtered by setting argument `manual.select=TRUE` and modifying logical values (`TRUE` or `FALSE`) in the second column (with column name `Selected`) of Fig. 2. This function re-orders the selected records according to their `Position` and `Grain`. To improve visibility and clarity, data records with different combination of `Position` and `Grain` are separated by two rows of blanks in the summary table (see Fig. 2). The output of function `pickBINdata()` is an object of S3 class "pickBIN".

2.2. Signal analysis

Data records stored in object "pickBIN" can be analysed using the function `analyseBINdata()`. A number of arguments are available to suit different types of data analysis.

2.2.1 Net OSL calculation

The first step of signal analysis is to select appropriate time integrals (or channels) to calculate the net OSL

Selected Records

File

	row.names	Selected	Position	Grain	Run	Set	DType	IRRTime	NPoints	LType	Low	High	Rate	Temperature	Delay	On	Off	LightSource	AnTemp	TimeSinceIrr	Time
1	6	TRUE	1	1	1	3	Natural	0	100	TRPOSL	0	2	5	0	5	90	5	GreenLaser	125	-1	82156
2	511	TRUE	1	1	1	6	Dose	100	100	TRPOSL	0	2	5	0	5	90	5	GreenLaser	125	-1	93021
3	1016	TRUE	1	1	2	3	Bleach+dose	600	100	TRPOSL	0	2	5	0	5	90	5	GreenLaser	125	-1	112308
4	1521	TRUE	1	1	2	6	Dose	100	100	TRPOSL	0	2	5	0	5	90	5	GreenLaser	125	-1	123142
5	2026	TRUE	1	1	3	3	Bleach+dose	1200	100	TRPOSL	0	2	5	0	5	90	5	GreenLaser	125	-1	31442
6	2531	TRUE	1	1	3	6	Dose	100	100	TRPOSL	0	2	5	0	5	90	5	GreenLaser	125	-1	114439
7	3036	TRUE	1	1	4	3	Bleach+dose	1800	100	TRPOSL	0	2	5	0	5	90	5	GreenLaser	125	-1	32543
8	3541	TRUE	1	1	4	6	Dose	100	100	TRPOSL	0	2	5	0	5	90	5	GreenLaser	125	-1	43640
9	4046	TRUE	1	1	5	3	Bleach+dose	2400	100	TRPOSL	0	2	5	0	5	90	5	GreenLaser	125	-1	90250
10	4551	TRUE	1	1	5	6	Dose	100	100	TRPOSL	0	2	5	0	5	90	5	GreenLaser	125	-1	101133
11	5056	TRUE	1	1	6	3	Bleach+dose	3200	100	TRPOSL	0	2	5	0	5	90	5	GreenLaser	125	-1	34153
12	5561	TRUE	1	1	6	6	Dose	100	100	TRPOSL	0	2	5	0	5	90	5	GreenLaser	125	-1	45022
13	6066	TRUE	1	1	7	3	Bleach+dose	0	100	TRPOSL	0	2	5	0	5	90	5	GreenLaser	125	-1	55258
14	6571	TRUE	1	1	7	6	Dose	100	100	TRPOSL	0	2	5	0	5	90	5	GreenLaser	125	-1	70152
15	7076	TRUE	1	1	8	3	Bleach+dose	600	100	TRPOSL	0	2	5	0	5	90	5	GreenLaser	125	-1	85437
16	7581	TRUE	1	1	8	6	Dose	100	100	TRPOSL	0	2	5	0	5	90	5	GreenLaser	125	-1	100323
17	8091	TRUE	1	1	10	3	Bleach+dose	600	100	TRPOSL	0	2	5	0	5	90	5	GreenLaser	125	-1	120220
18	8596	TRUE	1	1	10	6	Dose	100	100	TRPOSL	0	2	5	0	5	90	5	GreenLaser	125	-1	11059
19	-9																				
20	-10																				
21	7	TRUE	1	2	1	3	Natural	0	100	TRPOSL	0	2	5	0	5	90	5	GreenLaser	125	-1	82201
22	512	TRUE	1	2	1	6	Dose	100	100	TRPOSL	0	2	5	0	5	90	5	GreenLaser	125	-1	93026
23	1017	TRUE	1	2	2	3	Bleach+dose	600	100	TRPOSL	0	2	5	0	5	90	5	GreenLaser	125	-1	112312
24	1522	TRUE	1	2	2	6	Dose	100	100	TRPOSL	0	2	5	0	5	90	5	GreenLaser	125	-1	123147
25	2027	TRUE	1	2	3	3	Bleach+dose	1200	100	TRPOSL	0	2	5	0	5	90	5	GreenLaser	125	-1	31447
26	2532	TRUE	1	2	3	6	Dose	100	100	TRPOSL	0	2	5	0	5	90	5	GreenLaser	125	-1	114444
27	3037	TRUE	1	2	4	3	Bleach+dose	1800	100	TRPOSL	0	2	5	0	5	90	5	GreenLaser	125	-1	32547
28	3542	TRUE	1	2	4	6	Dose	100	100	TRPOSL	0	2	5	0	5	90	5	GreenLaser	125	-1	43644
29	4047	TRUE	1	2	5	3	Bleach+dose	2400	100	TRPOSL	0	2	5	0	5	90	5	GreenLaser	125	-1	90254
30	4552	TRUE	1	2	5	6	Dose	100	100	TRPOSL	0	2	5	0	5	90	5	GreenLaser	125	-1	101138
31	5057	TRUE	1	2	6	3	Bleach+dose	3200	100	TRPOSL	0	2	5	0	5	90	5	GreenLaser	125	-1	34158
32	5562	TRUE	1	2	6	6	Dose	100	100	TRPOSL	0	2	5	0	5	90	5	GreenLaser	125	-1	45026
33	6067	TRUE	1	2	7	3	Bleach+dose	0	100	TRPOSL	0	2	5	0	5	90	5	GreenLaser	125	-1	55302
34	6572	TRUE	1	2	7	6	Dose	100	100	TRPOSL	0	2	5	0	5	90	5	GreenLaser	125	-1	70156

Figure 2. Summary of the attributes of selected records using `pickBINdata()`, by setting the argument `view=TRUE`.

intensity. Two arguments `nfchn` and `nlchn` are used to specify the numbers of channels to be used for calculating initial signal and background, respectively. Two background subtraction methods, the "early" and "late" background subtraction, are available via setting the argument `bg='early'` or `bg='late'`, respectively. It is to be noted that this function automatically detects the start and end of signal based on the attributes `NPoints` (the total number of channels), `Delay` (the "light-off" channels before stimulation), and `Off` (the "light-off" channels after stimulation) of the corresponding signal record. This is useful when some channels have been allocated before or/and after stimulation; a "light-off" (or delay) period is commonly used to monitor any residual thermal signal after preheat (e.g., Fu et al., 2012). In this case, the signal channels are calculated as `(Delay+1):(Delay+nfchn)`, and the background channels for the "early" and "late" background subtraction methods are calculated as `(Delay+nfchn+1):(Delay+nfchn+nlchn)` and `(NPoints-Off-nlchn+1):(NPoints-Off)`, respectively.

2.2.2 Signal error estimation

The counting error of luminescence signal can be estimated using two methods. For the argument `distp='p'`, the variance of photon counts is assumed to follow a Poisson distribution. In this case, the relative standard error of the net OSL response (L) is estimated using the formula described by Galbraith (2002):

$$\mathrm{rse}(L) = \frac{\sqrt{I_f + \frac{t_f^2}{t_l^2} I_l}}{I_f - \frac{t_f}{t_l} I_l} \tag{1}$$

where I_f is the total number of counts over the first few channels of total duration t_f of the decay curve. I_l is the total number of counts over the last few channels of total duration t_l. However, recent studies (e.g., Li, 2007; Adamiec et al., 2012) suggest that the variation in photon counts are dispersed more than would be expected from the assumed Poisson distribution. In this case, the user can set the argument `distp='op'` to calculate the relative standard error following the equation provided by Bluszcz et al. (2015):

$$\mathrm{rse}(L) = \sqrt{k_{ph}^2 I_f + (k_{dc}^2 - k_{ph}^2)\dot{B}t_f + \frac{t_f^2}{t_l^2}(k_{ph}^2 I_l + (k_{dc}^2 - k_{ph}^2)\dot{B}t_l)} \frac{1}{I_f - \frac{t_f}{t_l} I_l} \tag{2}$$

where k_{ph} and k_{dc} are the square root of variance to mean ratio (Adamiec et al., 2012) for the photon and dark counts, respectively, and $\dot{B}$ denotes the dark count rate (unit in cts/s). It is noted that, to be able to use this method, the user need to provide the values of k_{ph}, k_{dc}, and $\dot{B}$ (through arguments `kph`, `kdc`, and `dcr`, respectively), which should be measured independently for individual readers or measurement systems (see Adamiec et al. 2012 for details), as argument inputs for the function `analyseBINdata()`. Then the relative standard error of sensitivity-corrected OSL (L/T) is estimated as:

$$\mathrm{rse}\left(\frac{L}{T}\right) = \sqrt{\mathrm{rse}^2(L) + \mathrm{rse}^2(T) + 2\sigma_{ins}^2} \tag{3}$$

where σ_{ins} is the instrumental irreproducibility for each individual OSL measurement (L or T) that can be set using the argument `me` in function `analyseBINdata()`.

2.2.3 Signal type selection

Apart from extracting the sensitivity-corrected signals (L/T), a default setting for the SAR procedure, user can also set the argument `signal.type` to extract the results of "L", or "T". This is useful for analysing the data from a procedure different from SAR, such as the pre-dose MET-pIRIR procedure for K-feldspar (Li et al., 2013, 2014), where the sensitivity-corrected (L/T), test dose (T) and sensitivity-uncorrected (L) signals can be used for D_e estimation.

2.2.4 Fast ratio of the signal

In the function `analyseBINdata()`, the user can also set the arguments `FR.fchn`, `FR.mchn` and `FR.lchn`, denoting the channels for fast component, medium component and background, respectively, to estimate the "fast ratio" (Durcan & Duller, 2011) for quantifying the dominance of the fast component in the initial test-dose response for the natural dose (T_n). Since the fast ratio will vary depending on the power density and wavelength of stimulation source being used for OSL measurements, the channel integrals used to determine it (i.e., `FR.fchn`, `FR.mchn`, `FR.lchn`) are set to `NULL` by default. So the fast ratio will not be calculated unless the values of `FR.fchn`, `FR.mchn`, `FR.lchn` are specified by the user.

2.2.5 Output signal analysis results

The function `analyseBINdata()` returns an invisible list of S3 class object "analyseBIN". The SAR data related quantities (such as the position and grain numbers, SAR cycles, doses, signals and backgrounds for each aliquot or grain, etc) can be output into a named CSV file via the argument `outfile`. Figure 3 shows an example of the quantities saved in a CSV file.

2.2.6 Comparing results of signal analysis with *Analyst*

Figure 4 compares sensitivity-corrected natural signal L_n/T_n and associated standard errors estimated using `'numOSL'` (version 2.3) and *Analyst* (version 4.31.9), using the single-grain data from sample HF11 from Haua Fteah (Cyrenaica, northeast Libya) (Douka et al., 2014; Li et al., 2016; Jacobs et al., 2017). The Pearson correlation coefficient $R^2 = 1$ indicates that L_n/T_n and associated standard errors (based on Poisson distribution) calculated using the two software packages are identical (Fig. 4A–B). However, since the counting statistics of the reader used to measure this sample does not follow a Poisson distribution (i.e., $k_{ph} = 1.37$ and $k_{dc} = 1.92$), the standard errors of L_n/T_n estimated using eqn. (2) are systematically larger than those estimated using eqn. (1) (Fig.4C); this suggests that the uncertainty of the sensitivity-corrected signal determined using eqn. (1) is likely to be underestimated when photon count numbers do not follow a Poisson distribution.

2.3. SAR D_e analysis

Function `calSARED()` calculates a series of SAR D_e values for different aliquots (grains) in a batch model using the data stored in the object "analyseBIN". Both D_e determination and rejection of unreliable D_e estimates can be achieved using this function.

2.3.1 Growth curve fitting

Fitting of the regenerative-dose data is implemented internally according to the Levenberg-Marquardt algorithm (Moré, 1978). In the function `calSARED()`, five models can be chosen for growth curve fitting via the argument `model`, including:

$$f(x) = ax + b \tag{4}$$

$$f(x) = a[(1 - exp(-bx)]) + c \tag{5}$$

$$f(x) = a[1 - exp(-bx)] + cx + d \tag{6}$$

$$f(x) = a[1 - exp(-bx)] + c[1 - exp(-dx)] + e \tag{7}$$

$$f(x) = a[1 - (1 + bcx)^{-1/c}] + d \tag{8}$$

Eqn. (4)–(8) describe the linear (LINE, `model='line'`), single saturation exponential (EXP, `model='exp'`), single saturation exponential plus linear (LEXP, `model='lexp'`), double saturation exponential (DEXP, `model='dexp'`), and general order kinetic model (GOK, `model='gok'`) (Guralnik et al., 2015), respectively. Where x and $f(x)$ denote regenerative dose and corresponding dose response signal, respectively, and a, b, c, d, e are parameters to be optimised. It is vitally important that the number of data points (N) to be fitted should at least be equal to the number of model parameters (n). The optimal parameters are obtained through "trial-and-error". Argument `weight` is a logical value indicating if the growth curve should be fitted using a weighted procedure (weighted by the inverse variance of individual data point). Argument `trial` is a logical value indicating if the growth curve should be fitted using other models if the given model fails. Growth curves can be fitted with more flexibility during the batch process by setting `trial=TRUE`. For example, if the fitting model is specified as LEXP, then a number of models (i.e., LEXP, GOK, EXP, LINE) will be tried one after another until the fit succeeds when `trial=TRUE`. In contrast, only the LEXP model will be tried if `trial=FALSE`.

The GOK model (Guralnik et al., 2015) is used by default in the function `calSARED()`. This model is highly recommended for batch analysis given its generality and robustness. In the GOK model, a denotes the maximum signal level, b is the reciprocal of the saturation dose D_0, c is a kinetic order modifier, and d is an offset accounting for potential "recuperation" effects. For $c \to 0$, the GOK model

A	B	C	D	E	F	G	H	I	J	K	L	M	N	O	P
	NO	Position	Grain	SAR.Cycle	Dose	Init	BG	Lx	seLx	TInit	TBG	Tx	seTx	LxTx	seLxTx
1	1	1	1	N	0	22642	524.5	22117.5	467.523	4258	127.5	4130.5	105.5754	5.354679	0.177605
2	1	1	1	R1	600	15736	340.5	15395.5	332.7384	3864	114.5	3749.5	97.69724	4.106014	0.139001
3	1	1	1	R2	1200	21926	532.5	21393.5	453.0618	4361	101	4260	108.0303	5.021948	0.16592
4	1	1	1	R3	1800	28159	687	27472	574.7928	5185	143	5042	124.1983	5.448631	0.176096
5	1	1	1	R4	2400	28918	809.5	28108.5	587.6716	5503	147.5	5355.5	130.573	5.24853	0.168571
6	1	1	1	R5	3200	34665	970	33695	699.4935	5989	171	5818	140.0505	5.791509	0.184095
7	1	1	1	R6	0	299	88.5	210.5	18.99932	6256	170	6086	145.4536	0.034588	0.003229
8	1	1	1	R7	600	20979	408	20571	436.4051	5726	197	5529	134.3594	3.720564	0.120019
9	1	1	1	R8	600	20843	426	20417	433.3562	5776	155.5	5620.5	135.977	3.632595	0.116912
10	2	1	2	N	0	51206	572.5	50633.5	1037.783	7136	150	6986	163.5013	7.247853	0.225481
11	2	1	2	R1	600	30530	349.5	30180.5	628.5299	6345	132	6213	147.8227	4.857637	0.153596
12	2	1	2	R2	1200	46353	555.5	45797.5	941.0607	7198	170.5	7027.5	164.431	6.516898	0.202937
13	2	1	2	R3	1800	57639	778	56861	1162.453	8425	191.5	8233.5	188.7775	6.906055	0.212145
14	2	1	2	R4	2400	67979	868.5	67110.5	1367.458	9165	213	8952	203.29	7.496705	0.228727
15	2	1	2	R5	3200	69506	986.5	68519.5	1395.696	9291	266	9025	204.9494	7.592188	0.231607
16	2	1	2	R6	0	566	120	446	26.5625	9419	210	9209	208.4377	0.048431	0.003086
17	2	1	2	R7	600	38278	454	37824	781.5158	8311	221.5	8089.5	186.0047	4.675691	0.144539
18	2	1	2	R8	600	37346	533	36813	761.3746	8651	199	8452	193.1968	4.355537	0.134264
19	3	1	3	N	0	13345	465	12880	282.7282	2556	128.5	2427.5	70.55035	5.30587	0.193246
20	3	1	3	R1	600	9780	351	9429	213.3493	2446	133	2313	68.20915	4.076524	0.151524
21	3	1	3	R2	1200	13021	495	12526	275.7332	2636	139.5	2496.5	72.10239	5.017424	0.182202
22	3	1	3	R3	1800	13904	597.5	13306.5	291.5955	2795	175.5	2619.5	75.01641	5.079786	0.183178
23	3	1	3	R4	2400	14878	630.5	14247.5	310.467	2894	179.5	2714.5	77.01399	5.248665	0.187766
24	3	1	3	R5	3200	15211	771	14440	314.6457	3001	230	2771	78.65988	5.211115	0.186483
25	3	1	3	R6	0	239	67.5	171.5	16.86757	2857	202.5	2654.5	76.00525	0.064607	0.006618
26	3	1	3	R7	600	9965	442	9523	215.5482	2682	172.5	2509.5	72.71373	3.79478	0.139527
27	3	1	3	R8	600	9448	450	8998	205.0819	2491	152	2339	68.95918	3.846943	0.143356
28	4	1	4	N	0	134804	503.5	134300.5	2711.034	17954	161.5	17792.5	380.3472	7.548152	0.221928

Figure 3. An example of the CSV file output by function `analyseBINdata()`. `Init` and `BG` denote the initial and background signals, respectively. `Lx=Init-BG`, `Tx=TInit-TBG`, `LxTx=Lx/Tx`, `seLx`, `seTx`, and `seLxTx` are the standard errors of `Lx`, `Tx`, and `LxTx`, respectively.

reduces to the EXP model, but as c increases, the GOK model progressively deviates from first-order behaviour and approximates the LEXP or DEXP model. Guralnik et al. (2015) demonstrated that the GOK model can successfully capture the behaviours of different materials and experimental conditions using a minimum number of model parameters.

The performance of the GOK model was tested and compared to other models using a large number of single-grain data sets from sample HF11, as shown in Fig.5. A total of 665 growth curves were fitted using different models. It turns out that the numbers of grains that fail in fitting are 0, 0, 310, and 237 for the EXP, GOK, LEXP, and DEXP models, respectively. This suggests that the universality and flexibility of EXP and GOK models are significantly better than the LEXP and DEXP models. The goodness-of-fit (see the next section) of the GOK model is marginally better than the EXP model (Fig. 5A–B) and comparable to the LEXP and DEXP models (Fig. 5C–F). Based on this comparison, we use GOK as a default fitting model for a batch analysis.

2.3.2 Goodness of fit

Two criteria are employed to measure the goodness-of-fit, i.e., the reduced chi-square (RCS) and figure-of-merit (FOM). The RCS is routinely provided in *Analyst* to measure the quality of fit of growth curves, which is defined as follows:

$$RCS = \frac{1}{N-n} \times \Sigma \frac{(y_i^o - y_i^f)^2}{\sigma_i^2} \tag{9}$$

where y_i^o and y_i^f denote the $i-th$ observed and fitted values, respectively, N and n denote the number of data points and the number of model parameters, respectively, and σ_i denotes the standard error for the $i-th$ observation. The value of RCS approximates unity if the fitting model is a good approximation of the observations (Bevington & Robinson, 2002). RCS greater than 1 indicates that the fitting function is not appropriate for describing the data points. However, a RCS less than 1 does not necessarily indicate a high-quality fit. A value of RCS that is very small may indicate overestimation of the uncertainties of observations (Bevington & Robinson, 2002) or an inappropriate assignment of fitting model.

The FOM is widely used to measure the goodness-of-fit in thermoluminescence (TL) glow curve deconvolution (Bos et al., 1994; Pagonis & Kitis, 2002). According to Balian & Eddy (1977), the FOM is defined as follows:

$$FOM = 100\% \times \frac{\Sigma |y_i^o - y_i^f|}{\Sigma y_i^f} \tag{10}$$

Balian & Eddy (1977) considered a good fit to have a FOM value of less than 2.5 %. Horowitz & Yossian (1995) suggested that a FOM value on the order of a few percent indicates an accurate fit for their computerized glow curves. According to our experience, the upper limit on FOM should not exceed 10%.

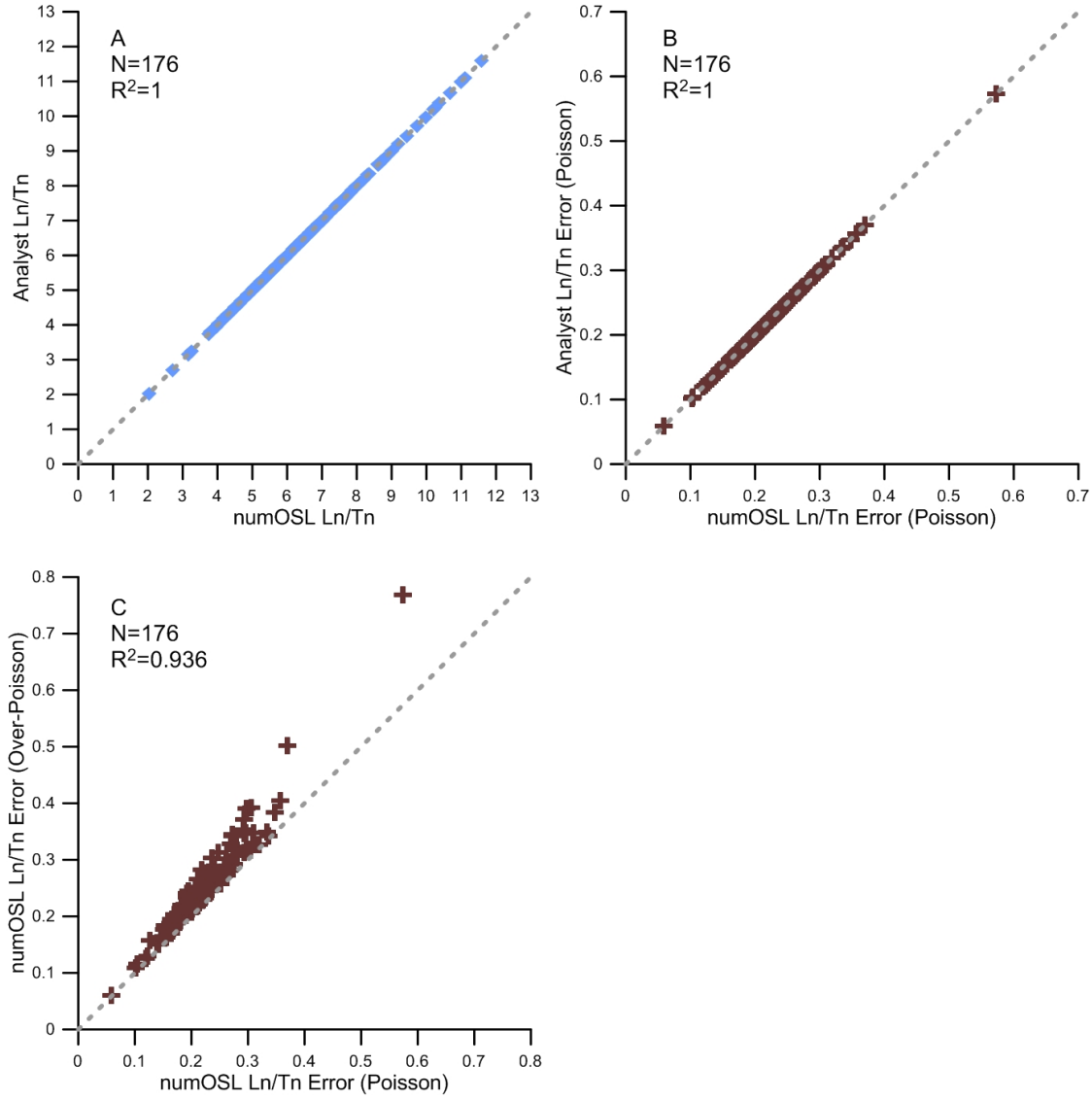

Figure 4. Comparison of L_n/T_n (A) and its standard error (B) calculated using `'numOSL'` and *Analyst*, using 176 grains from sample HF11. The net OSL was calculated using the "late" background subtraction method. The numbers of channels used for signal and background integration are 5 and 10, respectively. A relative standard error of 2% per measurement was combined in quadrature with the uncertainty of the net OSL by setting argument `me=2` in function `analyseBINdata()`. The dashed line indicates $y = x$. (C) Comparison of standard error of L_n/T_n estimated using Poisson and over Poisson distributions of photon counts. Correction factors were set as $k_{ph} = 1.37$ and $k_{dc} = 1.92$, and the dark count rate was set equal to 70 cts/s.

Both RCS and FOM have their own advantages and disadvantages as a measurement of goodness-of-fit of growth curves. Firstly, the RCS takes the standard errors of observations into consideration, while the FOM takes only the differences between observed and fitted data into account. For dim samples where large counting uncertainties are associated with the measured signals, large scatter may be expected for their growth curves. In this case, the growth curve under analysis may yield small RCS but large FOM. On the contrary, a bright sample may have well-behaved growth curves that can yield small fitting residuals (or FOM values) but high RCS values (due to the small error in signal). Secondly, the differences between the observed and fitted data are normalised using the fitted data in FOM, but this is not the case for RCS. Such a normalisation has an advantage to avoid the problem that the difference between the observed and fitted values increases with the size of observed values. As a result, FOM is more appropriate for comparing the quality of fit between growth curves that have significantly different magnitudes in signal intensity. Finally, according to Eqn. (9), RCS is only suitable for cases where the numbers of data points N is larger than the number of model parameters n. According to our experience, most of the growth curves with a RCS value below 5 and a FOM value below 10 may have an satisfactory fit; the user can, however, set a more stringent criterion by using smaller RCS and FOM values.

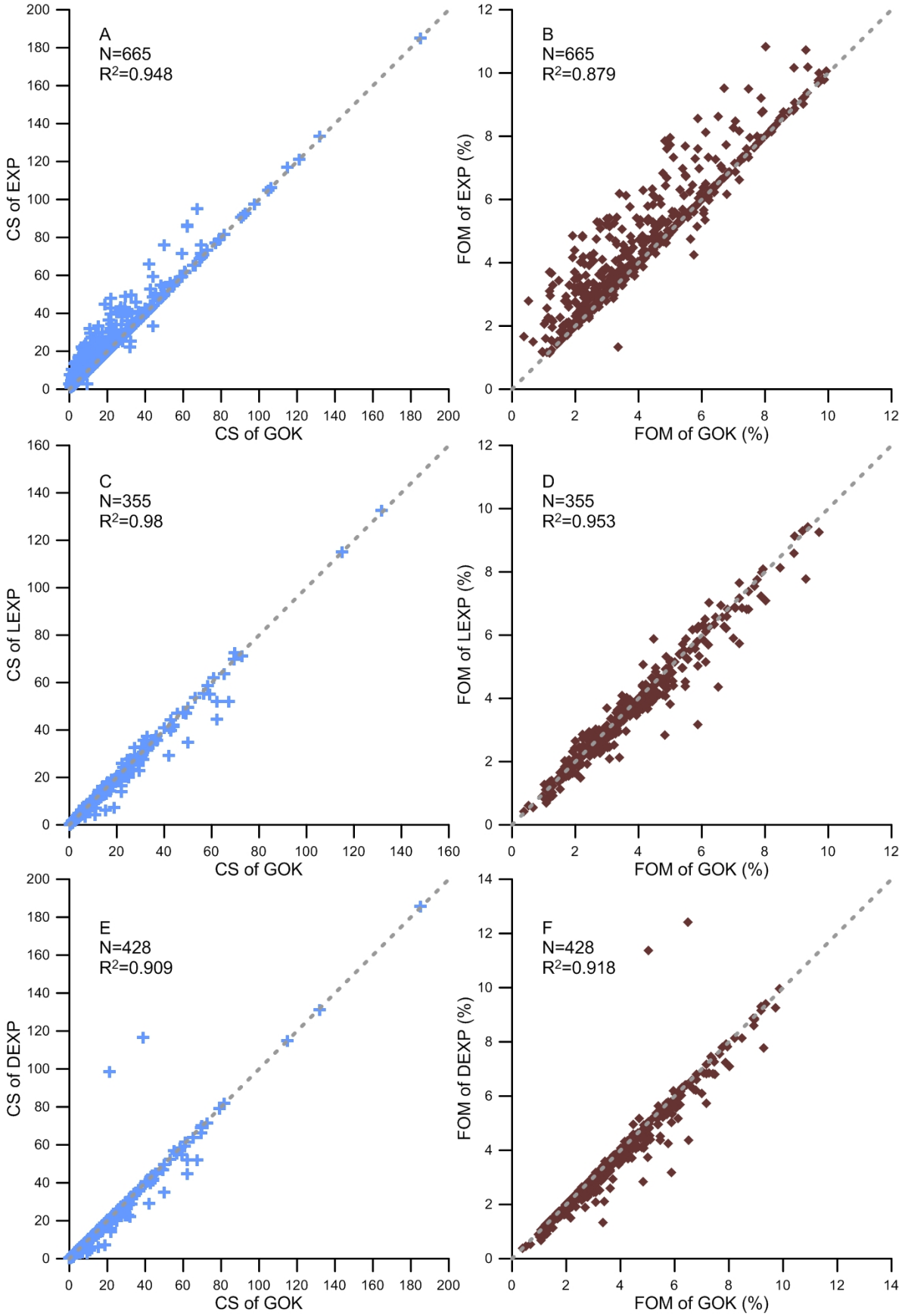

Figure 5. Comparison of goodness-of-fits between the GOK model and the EXP, LEXP, DEXP models. CS and FOM are short for chi-square and figure-of-merit values, respectively. The dashed line indicates $y = x$.

2.3.3 Error estimation in D_e

The function `calSARED()` employs two methods proposed by Duller (2007) to estimate the standard error of D_e estimate, i.e., simple transformation and Monte Carlo simulation (also called a "parameter bootstrap" method) by specifying the argument `errMethod`. For the simple transformation method used in *Analyst*, the standard error of the natural signal is combined in quadrature with the uncertainty of the fitted growth curve (i.e., the average deviation between observed and fitted data) (Duller, 2007):

$$avgDev = \frac{\sqrt{\Sigma_{i=1}^{i=N}(y_i^0 - y_i^f)^2}}{N} \tag{11}$$

This combined error is then propagated through interpolation on the growth curve to calculate the lower and upper limits on the D_e estimate and associated error. The simple transformation method takes less calculation resource and is less time-consuming compared to the Monte Carlo method. It should be mentioned that a finite upper limit on D_e cannot be obtained if the natural signal (L_n/T_n) is statistically consistent with, or above, the saturation level of the growth curve, indicating that the natural signal of the aliquot (grain) may have been saturated. When the simple transformation method is used, the function `calSARED()` estimates D_e error as well as its 68 (one sigma) and 95% (two sigma) confidence intervals by assuming that the sampling distribution of D_e is approximately normal (Galbraith & Roberts, 2012).

For the Monte Carlo method, the assessment of standard error of D_e estimate involves calculating a number of D_e values by randomly generating natural and regenerative signals according to Gaussian distributions. The 68% and 95% confidence intervals of D_e are derived directly from the sampling distribution of randomly simulated D_e. This method provides more reliable confidence interval estimates, especially when the sampling distribution of D_e is not approximately normal. It must be pointed out, however, that, when the natural signal lies on the non-linear region of a saturating exponential growth curve, the distribution of randomly simulated D_e using the Monte Carlo method tends to have an asymmetric distribution. As a result, the distribution of randomly simulated D_e may be significantly truncated if $D_e > 2D_0$ (D_0 denotes the characteristic saturation dose in a saturating exponential function) (or L_n/T_n exceeds about 85% of the saturation level). This is because many of the randomly simulated natural signals may not intersect the corresponding growth curve. In this situation, both the mean random D_e and the D_e error are likely to be underestimated.

2.3.4 SAR D_e selection using rejection criteria

In OSL dating, it is important to select aliquots (grains) that are suitable for D_e determination. Potential rejection criteria can be divided into several categories, including (1) signal-related criteria, such as whether the test-dose response for the natural dose (T_n) is more than 3 sigma above the background (BG) (Jacobs et al., 2006), ratio of initial signal to BG for T_n, relative standard error of T_n (Ballarini et al., 2007), and fast ratio of T_n (Madsen et al., 2009; Durcan & Duller, 2011; Duller, 2012); (2) growth-curve-related criteria, such as recycling ratio (Wintle & Murray, 2006), OSL-IR depletion ratio (Duller, 2003), recuperation (Wintle & Murray, 2006), and goodness of fit; (3) D_e-related criteria, such as the methods used for D_e determination (interpolation or extrapolation), relative standard error of D_e, etc.

We have incorporated a range of rejection criteria for extracting reliable D_e estimates in the function `calSARED()`, including (a) `Tn.above.3BG`: if the net test-dose OSL response for the natural dose (T_n) is 3 sigma above the background; (b) `TnBG.ratio.low`: lower limit on the ratio of initial signal to background for T_n; (c) `rseTn.up`: upper limit on the relative standard error of T_n; (d) `FR.low`: lower limit on the fast ratio of T_n; (e) `rcy1.range`, `rcy2.range`, and `rcy3.range`: lower and upper limits on recycling ratios (note that only the first three identical doses are taken into account); (f) `rcp1.up` and `rcp2.up`: upper limits on recuperation (note that `rcp1` and `rcp2` are the ratios of the sensitivity-corrected zero-dose signal to natural signal and to the signal from the maximum regenerative dose, respectively); (g) `fom.up`: upper limit on the FOM of fitted growth curve; (h) `rcs.up`: upper limit on the RCS of fitted growth curve; (i) `calED.method`: the method used for D_e determination (interpolation or extrapolation); (j) `rseED.up`: upper limit on the relative standard error of D_e. Among the rejection criteria listed above, (a)–(d) are signal-related, (e)–(h) are growth-curve-related, and (i)–(j) are D_e-related. Argument `use.se` is a logical value indicating if standard errors (two sigma) are taken into consideration during application of rejection criteria. Note that the user does not have to specify arguments for all the rejection criteria listed above. If the user does not want to consider a particular rejection criterion then they can simply leave the argument out of the function.

It should be noted that if the sensitivity-corrected signals for the first, second, and third repeated regenerative doses are L_{r_1}/T_{r_1}, L_{r_2}/T_{r_2}, and L_{r_3}/T_{r_3}, respectively, then the first, second and third recycling ratios are calculated as $[L_{r_2}/T_{r_2}]/[L_{r_1}/T_{r_1}]$, $[L_{r_3}/T_{r_3}]/[L_{r_1}/T_{r_1}]$, and $[L_{r_3}/T_{r_3}]/[L_{r_2}/T_{r_2}]$ (similar to *Analyst*). The lower and upper limits on recycling ratios can be specified directly by the user to apply recycling ratio criteria. In contrast, the application of the OSL-IR depletion ratio criterion is not straightforward. For example, if three duplicate regenerative doses are administrated and OSL responses from the first two regenerative doses are measured without infrared stimulation while only the 3rd one is measured after being exposed to infrared stimulation, then the OSL-IR depletion ratio will be calculated using the third recycling ratio (i.e., $[L_{r_3}/T_{r_3}]/[L_{r_2}/T_{r_2}]$. In this case, the user needs to specify argument `rcy3.range` to apply the OSL-IR depletion ratio criterion.

The function `calSARED()` calculates two recuperation ratios: the first ("recuperation-1") is the ratio of the sensitivity-corrected zero-dose to natural signals ($[L_0/T_0]/[L_n/T_n]$), which is commonly adopted as a measure of extent of thermal transfer (Murray & Wintle, 2000). However, for young

samples whose natural doses are close to zero or sensitivity-corrected natural signals are close to background, applying a low limit on "recuperation-1" may result in many grains (aliquots) being rejected. This may bias the results towards acceptance of older grains or aliquots whose natural signal are higher, and, hence, may overestimate the final D_e results. In this case, therefore, it is more reasonable to use "recuperation-2", the ratio of the zero-dose signal to that of the maximum regenerative dose ($[L_0/T_0]/[L_{max}/T_{max}]$), as an indicator of the extent of thermal transfer.

The function `calSARED()` was designated according to the principle that calculation resources should be saved as much as possible. For this purpose, signal-related rejection criteria (a–d) are applied firstly, and those aliquots (grains) rejected by these criteria will not be considered during the next step of analysis. The growth-curve-related criteria (e–h) are then applied to the culled data set, before the D_e-related criteria (i–j) are applied to any remaining aliquots (grains). The function returns a summary table (as shown in Fig. 6) showing the numbers of aliquots (grains) rejected by each of the specified rejection criterion and the number of aliquots (grains) that cannot be successfully calculated using function `calED()` (such as, improper input arguments, failure in growth curve fitting, saturation in natural signal, failure in D_e calculation or D_e error estimation, etc). Providing such a summary table is crucial, as it reveals the variability of luminescence behaviours of different grains or aliquots, and it has been widely used as the standard output information in single-grain dating (e.g. Feathers, 2003; Jacobs et al., 2006, 2015; Armitage et al., 2011; Arnold et al., 2012).

2.3.5 Output SAR D_e analysis results

The function `calSARED()` provides two arguments to output SAR D_e analysis results. The results of SAR D_e determination obtained through the batch process can be output graphically into a named PDF file via the argument `outpdf`. The SAR D_e related quantities (such as the position and grain numbers, values of rejection criteria, natural signal and associated standard error, standard error and confidence intervals of each accepted D_e estimate, etc.) can be output into a named CSV file via the argument `outfile`.

2.3.6 Comparing results of SAR D_e determination with *Analyst*

Figure 7 shows comparison between the D_e estimates and their associated standard errors determined using `'numOSL'` and*Analyst*, for single grains of sample HF11. The results obtained using the simple transformation method are indistinguishable ($R^2 = 1$) between the two software packages (Fig.7A–B). The D_e errors estimated using the Monte Carlo method are also consistent with each other ($R^2 = 0.974$) (Fig. 7C).

2.4. SGC D_e analysis

2.4.1 Select growth curves to establish SGC

SGC should be established using only those aliquots (grains) considered to be well-behaved so that reliable growth curves are produced (Li et al., 2016). Accordingly, poorly-behaved grains (aliquots) should be identified and rejected beforehand. In order to achieve this, function `pickSARdata()` uses rejection criteria similar to (but with exclusion of the D_e-related criteria) those used in function `calSARED()` to enable the user to select well-behaved grains or aliquots to establish SGC. The input of the function is an object "analyseBIN" produced by function `analyseBINdata()`. In order to save calculation resources, the design of function `pickSARdata()` is similar to the function `calSARED()`.

It is noted that, for single-grain quartz, different grains may have considerably different growth curve shapes (Li et al., 2016), which may prevent the establishment of a common SGC for all the grains. For such samples, Li et al. (2016) found that growth curves from different grains for their samples from Haua Fteah (Cyrenaica, northeast Libya) can be divided into three broad groups (i.e., "early", "medium" and "later"), with each group saturating at a different dose level. Each group of grains, however, share a common SGC, and the SGCs from different groups are identical up to a dose of 50 Gy after which they start to significantly deviate. Therefore, it is necessary to characterise the growth curves from different aliquots (grains) to check whether it is appropriate to establish a common SGC for the samples under consideration.

2.4.2 LS-normalisation

In comparison to the original SGC method from Roberts & Duller (2004) and the re-normalisation method from Li et al. (2015a,b), the LS-normalisation method of Li et al. (2016) can further reduce the variation of growth curves between aliquots (grains) measured from the same or different samples. This has been validated not only experimentally using natural sedimentary samples (Li et al., 2016) but also confirmed theoretically by modeling and simulation (Peng et al., 2016).

According to Li et al. (2016), the LS-normalisation procedure for SGC optimization involves the following steps: (1) fit regenerative-dose signals from all aliquots (grains) using a best-fit model (e.g., single saturating exponential function); (2) re-scale regenerative-dose signals from each aliquot (grains) using scaling factors determined in a way such that the difference between the re-scaled sensitivity-corrected regenerative-dose signals and the fitted common growth curve is minimised through an optimization procedure; each aliquot (grain) is treated individually, and different scaling factors are determined for different aliquots (grains); (3) repeat the fitting (step 1) and re-scaling (step 2) procedures iteratively. The iteration is performed repeatedly until there is negligible change in the relative standard deviation of re-scaled regenerative-dose signals.

	Description	N
1	Total number of analyzed aliquots (grains)	500
2	Rejection criterion: Tn below 3 sigma BG	0
3	Rejection criterion: ratio of Tn to BG below 3	0
4	Rejection criterion: RSE of Tn exceeds 30%	0
5	Rejection criterion: recycling ratio 1 outsides [0.9,1.1]	37
6	Rejection criterion: recycling ratio 3 outsides [0.9,1.1]	18
7	Rejection criterion: recuperation 2 exceeds 5%	0
8	Rejection criterion: FOM of growth curve exceeds 10%	80
9	Rejection criterion: RCS of growth curve exceeds 5	70
10	Rejection criterion: ED not calculated by Interpolation	7
11	Function calED(): improper input argument	0
12	Function calED(): failed in growth curve fitting	52
13	Function calED(): saturated in Ln/Tn	92
14	Function calED(): failed in ED calculation	0
15	Function calED(): failed in ED error estimation	0
16	Total number of rejected aliquots (grains)	356
17	Total number of accepted aliquots (grains)	144

Figure 6. A summary of results of SAR D_e analysis for 500 grains of sample HF11 reported from function `calSARED()`. Numbers of grains rejected according to user-supplied criteria and numbers of grains that cannot be successfully analysed using function `calED()` are summarised.

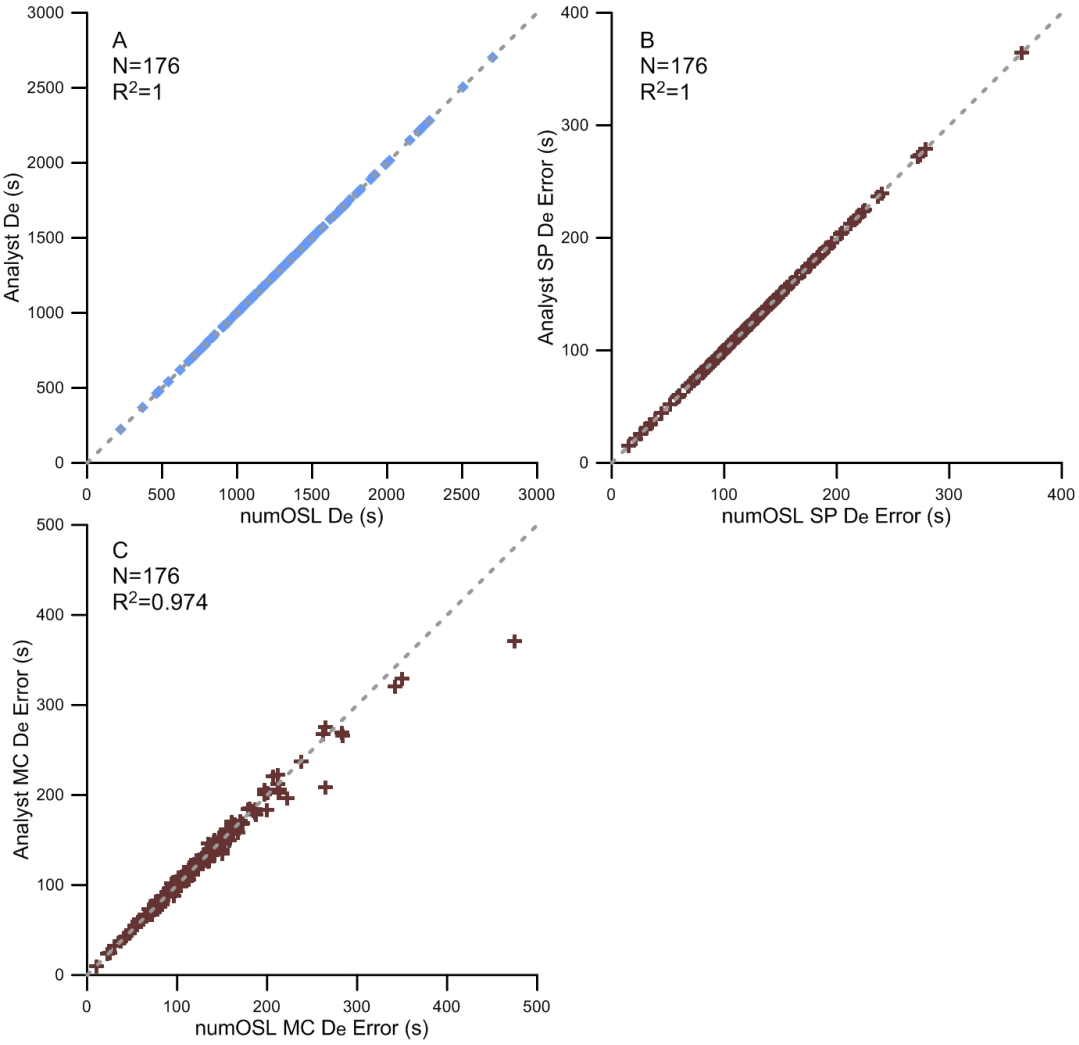

Figure 7. Comparison between SAR D_e values and associated standard errors obtained using '`numOSL`' and *Analyst*, using 176 single grains from sample HF11. The dashed line indicates $y = x$. Note that the unit of D_e is in irradiation time (second) rather than in Gy.

Li et al. (2016) found that the re-scaled regenerative-dose signals for the "early" group of their samples were best fitted using the EXP model, whereas those for the "medium" and "later" groups were best described using the DEXP model. They proposed that the best-fit model can be chosen on the basis of a chi-squared statistical test. However, during the application of this method, one needs to apply all possible models (such as LINE, EXP, LEXP, and DEXP) one after the other to the data to find out the best-fit model that yields the lowest chi-square value. For large data sets, the process is tedious and time-consuming. The function `lsNORM()` avoids the problem by applying the GOK model to fitting the data during the LS-normalisation process by default. The kinetic order modifier c in the GOK model (see eqn. (8)) automatically adjusts its magnitude to capture the variation pattern of the data during the fitting process.

We tested the performance of the function `lsNORM()` using randomly simulated growth curve data according to the kinetic model of Bailey (2001). The simulation was implemented using the **R** program KMS (Peng & Pagonis, 2016). The simulation steps are similar to those summarised in the Table 2 of Peng et al. (2016). The experimentally observed variability in OSL characteristics of quartz grains was simulated by allowing trap concentrations to vary randomly within $\pm 60\,\%$ of the original kinetic parameters of Bailey (2001), using uniformly distributed random numbers. Growth curves were simulated using regenerative doses of $0.4D_n$, $0.8D_n$, $1.2D_n$, $1.6D_n$, 0, and $0.4D_n$ Gy, where D_n stands for the natural dose and was simulated uniformly between 0 Gy and 200 Gy. The test dose was simulated uniformly from discrete numbers $[0.1D_n, 0.15D_n, 0.2D_n, 0.25D_n]$. The natural and laboratory dose rates were simulated uniformly from discrete numbers $[1\times10^{-3}, 1\times10^{-5}, 1\times10^{-7}, 1\times10^{-9}, 1\times10^{-11}]$ and $[0.2, 0.4, 0.6, 0.8, 1.0]$ Gy/s, respectively. The pre-heat and cut-heat temperatures were simulated uniformly from discrete numbers $[240, 250, 260]$ and $[200, 210, 220]\,^{\circ}$C, respectively.

The simulation result using 300 versions of model variants is shown in Fig.8A. It demonstrates that growth curve data simulated using various series of regenerative doses, test doses, natural and laboratory dose rates, and pre-heat and cut-heat temperatures show significantly difference in their shapes and magnitudes. The scatter of the data reduced significantly after being standardised using their test doses (Fig.8B). The variability of the data further decreased after being re-normalised using the sensitivity-corrected regenerative-dose signal at 200 Gy (Fig. 8C). The growth curve data re-scaled using the function `lsNORM()` demonstrate the lowest variability and best quality of fit (Fig. 8D).

It should be pointed out that, though the re-normalisation procedure of Li et al. (2015a,b) further reduces the scatter of growth curve data compared to the original SGC method of Roberts & Duller (2004), the application of the re-normalisation requires administration of a common regenerative dose (200 Gy in Fig. 8C) for different grains or aliquots. As a result, it is inapplicable if the growth curves used for SGC establishment do not share one common regenerative dose. In contrast, the LS-normalisation procedure of Li et al. (2016) does not require a common regenerative dose among all growth curves. This means that the normalisation can be implemented in a more flexible manner and it is possible to obtain more optimal results.

2.4.3 SGC D_e determination

Once a common SGC has been established, the sensitivity-corrected natural signal should be multiplied by a scaling factor, determined from the established SGC and an additional sensitivity-corrected regenerative-dose signal, to obtain the re-scaled natural signal in order to calculate a SGC D_e using the following formula:

$$\frac{L'_n}{T'_n} = \frac{L_n}{T_n} \times \frac{f(D_r)}{\frac{L_r}{T_r}} \tag{12}$$

where L'_n/T'_n denotes the re-scaled sensitivity-corrected natural signal, D_r and L_r/T_r denote the additional regenerative dose used for normalisation and the corresponding sensitivity-corrected signal, respectively, and $f(D_r)$ denotes the signal of D_r predicted using SGC established by LS-normalisation.

Function `calSGCED()` calculates D_e using the parameters (supplied using the argument `SGCpars`) of the SGC established externally through the function `lsNORM()` or `fitGrowth()`. D_e values can be calculated using the original SGC method proposed by Roberts & Duller (2004) (if argument `method='SGC'`) and the improved SGC method suggested by Li et al. (2016) (if argument `method='gSGC'`). Unlike function `calSARED()`, only signal-related rejection criteria can be used to select reliable D_e estimates in function `calSGCED()`.

The simple transformation method (rather than the Monte Carlo method) is implemented in function `calSGCED()` to assess error estimate of SGC D_e by default. During the application of the simple transformation method, the average deviation of established common SGC calculated according to eqn (11) is combined in quadrature with the uncertainty of the natural signal to account for the uncertainty of the SGC. This error term was taken into account via argument `avgDev`. The results of SGC D_e determination obtained through the batch process can also be output graphically into a named PDF file via the argument `outpdf`.

3. Worked examples

In this section, detailed examples for SAR and SGC D_e analysis are presented using **R** code templates. These templates are available from the supplementary and can be easily adapted by users for their own D_e analysis.

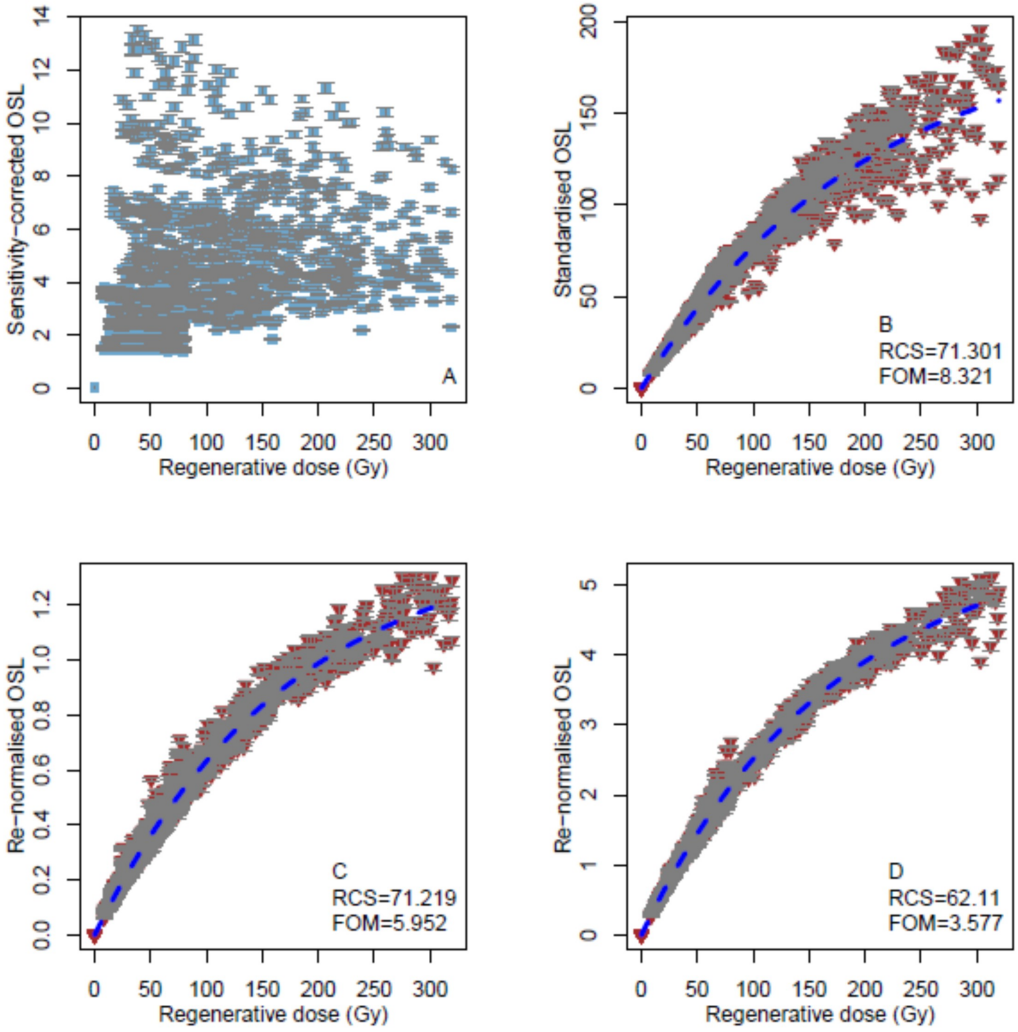

Figure 8. (A) Distribution of 300 randomly simulated growth curve data sets. Data shown in (B) was obtained by standardising the data from (A) using their corresponding test doses D_t. Data shown in (C) was obtained by re-normalising the data from (A) using sensitivity-corrected regenerative-dose signals at 200 Gy. Data shown in (D) was obtained by re-scaling the data from (A) using the LS-normalisation procedure. The dashed blue lines indicate the best-fit curves obtained using the GOK model.

3.1. SAR D_e determination and rejection criteria application

We first load package 'numOSL' into the **R** console using the first line of command (#1). BIN file "HF11(SG_Qtz_500_Grains).BIN" (available in the supplementary material) contains 500 grains of quartz OSL results for sample HF11. The file was loaded using function `loadBINdata()` and saved in object `res_loadBINdata` according to the commands in lines 2–3. The user needs to ensure that the BIN or BINX files to be imported are located in the current working directory. Imported single-grain data stored in `res_loadBINdata` with luminescence type of "TRPOSL" were selected using function `pickBINdata()` according to the commands in lines 4–6.

```
1 library(numOSL)
2 res_loadBINdata <- loadBINdata(
3  "HF11(SG_Qtz_500_Grains).BIN")
4 res_pickBINdata <- pickBINdata(
5  res_loadBINdata,
6  LType="TRPOSL")
```

Extracted data records stored in object `res_pickBINdata` were analysed using the function `analyseBINdata()` (the code in lines 7–13). The numbers of signal and background channels were set equal to 5 and 10, respectively (`nfchn=5`, `nlchn=10`). The "late" background subtraction method was used for net signal calculation (`bg='late'`). A measurement error of 2 % was given on each OSL measurement (i.e., L or T) (`me=2`). The photon counts were assumed to follow a Poisson distribution (`distp='p'`). Argument `signal.type='LxTx'` means that the sensitivity-corrected signal (L/T) was extracted. Results saved in a CSV file named "analyseBIN.csv" (available in the supplementary material) were output to the current work-

ing directory by using argument `outfile='analyseBIN'`.

```
7  res_analyseBINdata <-
8   analyseBINdata(
9   res_pickBINdata, nfchn=5,
10  nlchn=10, bg="late",
11  me=2, distp="p",
12  signal.type="LxTx",
13  outfile="analyseBIN")
```

Resultant data stored in object `res_analyseBINdata` were used to perform SAR D_e analysis using function `calSARED()` (code in lines 14–25). The GOK model was used and all growth curves were not forced to pass the origin (`model='gok'`, `origin=FALSE`). The Monte Carlo method was used for D_e error assessment and the desired number of simulation was set equal to 500 (`errMethod='mc'`, `nsim=500`), i.e., simulation will be performed repeatedly until 500 random D_e are generated. The acceptance rate of the Monte Carlo simulation is defined as the ratio of the number of obtained D_e to the total number of simulations. For example, if 1,000 simulations are performed and only 500 random D_e values are generated, then the acceptance rate of the simulation is 50 %. A low acceptance rate may imply that the model is not appropriate to fit the growth curve or the natural signal (L_n/T_n) is close to saturation; in the latter case a large number of simulated natural signals do not intersect with the simulated growth curves, so finite D_e cannot be obtained. Argument `trial=TRUE` ensures that other models will be tried if the given model fails in growth curve fitting.

Three signal-related rejection criteria (`Tn.above.3BG`, `TnBG.ratio.low`, and `rseTn.up`), five growth-curve-related criteria (`rcy1.range`, `rcy3.range`, `rcp2.up`, `fom.up`, and `rcs.up`), and one D_e-related criterion (`calED.method`) were then applied to select acceptable D_e values. Standard errors were taken into account during the application of rejection criteria (`use.se=TRUE`). The result of SAR D_e calculation was output to a PDF file named "calSARED.pdf" and a CSV file named "calSARED.csv" (`outpdf='calSARED'`, `outfile='calSARED'`) (available in the supplementary material). The SAR D_e analysis result for a grain of sample HF11 is shown in Fig. 9. A total of 356 grains were rejected according to these rejection criteria and 144 D_e values were obtained (as summarised in Fig. 6).

```
14 res_calSARED <- calSARED(
15   res_analyseBINdata,
16   model="gok", origin=FALSE,
17   errMethod="mc", nsim=500,
18   trial=TRUE, Tn.above.3BG=TRUE,
19   TnBG.ratio.low=3, rseTn.up=30,
20   rcy1.range=c(0.9,1.1),
21   rcy3.range=c(0.9,1.1),
22   rcp2.up=5, fom.up=10, rcs.up=5,
23   calED.method="Interpolation",
24   use.se=TRUE, outpdf="calSARED",
25   outfile="calSARED")
```

The calculated SAR D_e distribution for the 144 grains was visualized using a simplified (pseudo) radial plot (Galbraith, 1988) implemented using function `psRadialPlot()` from the `'numOSL'` package (the code in lines 26–29) (Fig. 10). The lower and upper limits on the z-axis are controlled by the arguments `zmin` and `zmax`, respectively.

```
26 psRadialPlot(
27   res_calSARED$sarED,
28   zmin=450, zmax=2100,
29   zlabel="De (s)")
```

3.2. Growth curve selection, LS-normalisation, and SGC D_e determination

BIN file "SA_Qtz_example.BIN" (available in the supplementary material) contains 24 multiple-grain aliquots of quartz OSL results for a fluvial sample from Shanxi province in China. The file was loaded and OSL data was selected using the commands in lines 30–31 and 32–33, respectively. Then we analysed the signal data using the **R** command in lines 34–38. We use function `pickSARdata()` to select well-behaved growth curves from data object `res_analyseBINdata1` using the commands in lines 39–47. Three signal-related criteria (`Tn.above.3BG`, `TnBG.ratio.low`, and `rseTn.up`) and four growth-curve-related criteria (`rcy1.range`, `rcp1.up`, `fom.up`, and `rcs.up`) were applied to select well-behaved growth curves. The results are output into a PDF file named "pickSARdata.pdf" (available in the supplementary material). Figure 11 shows results output by the function `pickSARdata()` for an aliquot of this sample.

```
30 res_loadBINdata1 <- loadBINdata(
31  "SA_Qtz_example.BIN")
```

```
32 res_pickBINdata1 <- pickBINdata(
33  res_loadBINdata1, LType="OSL")
```

```
34 res_analyseBINdata1 <-
35   analyseBINdata(
36   res_pickBINdata1, nfchn=10,
37   nlchn=20, bg="late", me=2,
38   distp="p", signal.type="LxTx")
```

```
39 res_pickSARdata <- pickSARdata(
40   res_analyseBINdata1,
41   model="gok", origin=FALSE,
42   Tn.above.3BG=TRUE,
43   TnBG.ratio.low=3, rseTn.up=30,
44   rcy1.range=c(0.9,1.1),
45   rcp1.up=10, fom.up=10,
46   rcs.up=5, use.se=TRUE,
47   outpdf="pickSARdata")
```

We use commands in lines 48–51 to optimise the selected growth curve data from well-behaved aliquots stored in `res_pickSARdata$SARdata` according to the LS-normalisation procedure using function `lsNORM()`. The allowed maximum number of iterations is set equal to 10 (`maxiter=10`). The automatically generated plot is shown in Fig. 12.

```
48 res_lsNORM <- lsNORM(
49  res_pickSARdata$SARdata,
50  model="gok", origin=FALSE,
51  maxiter=10)
```

The commands in lines 52–61 were used to calculate SGC D_e according to the method of Roberts & Duller (2004). Objects `res_lsNORM$LMpars1[,1]` and

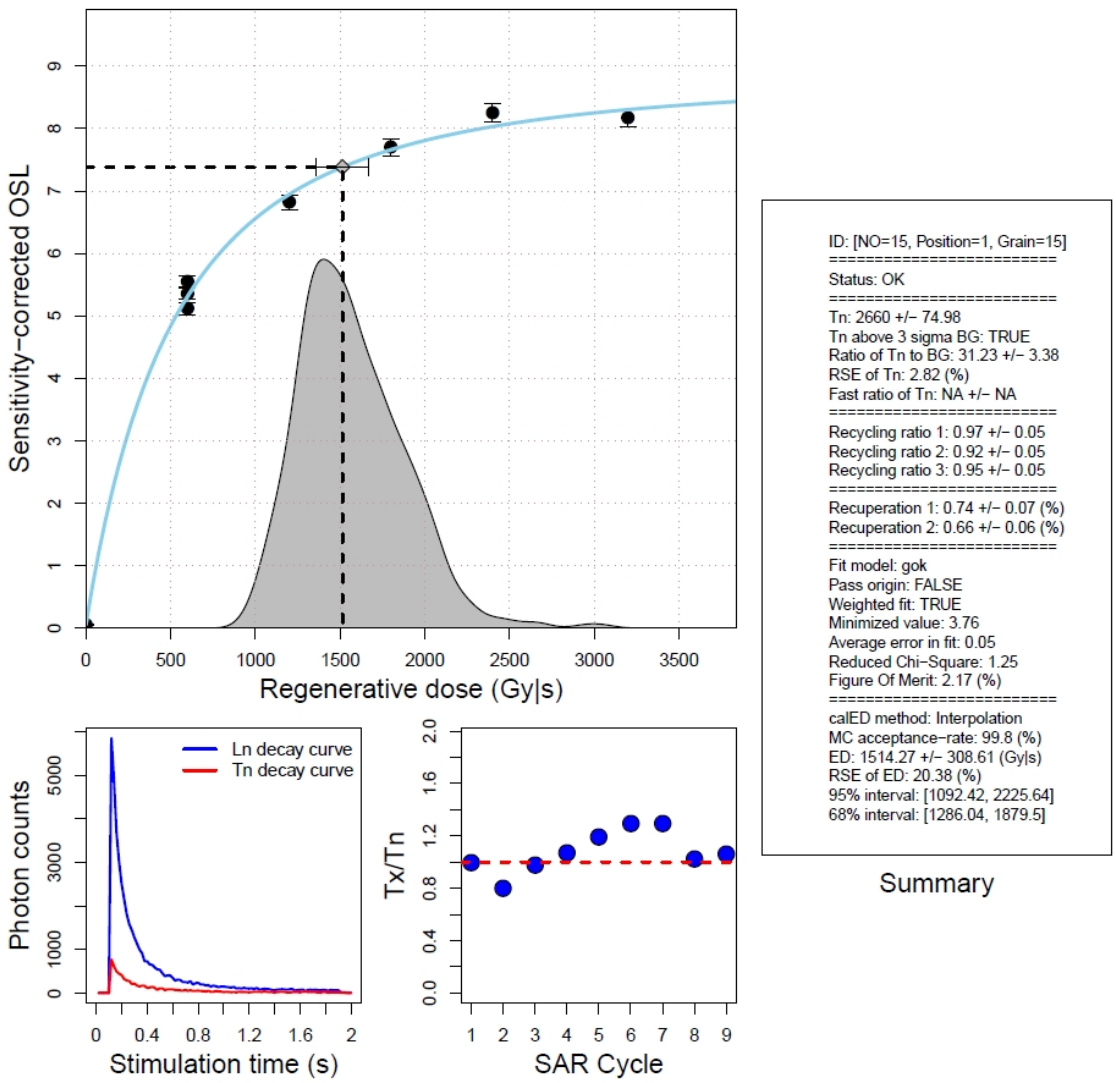

Figure 9. Results of SAR D_e calculation produced using function `calSARED()` for one of the grains of sample HF11.The upper plot shows results of growth curve fitting, D_e determination, and D_e error assessment using the Monte Carlo method. The distribution of the simulated D_e is shown in the grey area. The lower left plot shows the decay curves for the natural dose and its test dose. The lower right plot demonstrates the variation in the ratio of T_x to T_n for different SAR cycles. The right panel summarises the results of D_e calculation. The 68 % (one sigma) and 95 % (two sigma) confidence intervals of D_e were determined from the sampling distribution of randomly simulated D_e using the Monte Carlo method. Note that the unit of dose is in irradiation time (second) rather than in Gy.

`res_lsNORM$avg.error1` stand for the parameters and average deviation of the common SGC, respectively, established using growth curve data that have not been re-scaled by LS-normalisation. `res_lsNORM$LMpars1` is a two-column matrix in which SGC parameters and associated standard errors are stored in the first and second column, respectively. SGC parameters stored in the first column are accessed using `res_lsNORM$LMpars1[,1]`. The average deviation was used to account for uncertainty of the SGC, which was incorporated into the estimation of D_e error using the simple transformation method. It is of vital importance that arguments `model` and `origin` used in function `calSGCED()` are consistent with those used in function `lsNORM()`if the same parameters used in function `calSGCED()` are derived from the output of function `lsNORM()`. Three signal-related criteria (`Tn.above.3BG`, `TnBG.ratio.low`, and `rseTn.up`) were employed to select acceptable SGC D_e estimates (note that growth-curve-related criteria are inapplicable for the SGC method). The results of SGC D_e calculation were output into a PDF file named "SGCED.pdf" (available in the supplementary material).

```
res_SGCED <- calSGCED(
  res_analyseBINdata1,
  SGCpars=res_lsNORM$LMpars1[,1],
  model="gok", origin=FALSE,
  avgDev=res_lsNORM$avg.error1,
  method="SGC", errMethod="sp",
  SAR.Cycle="N",
  Tn.above.3BG=TRUE,
  TnBG.ratio.low=3, rseTn.up=30,
  use.se=TRUE, outpdf="SGCED")
```

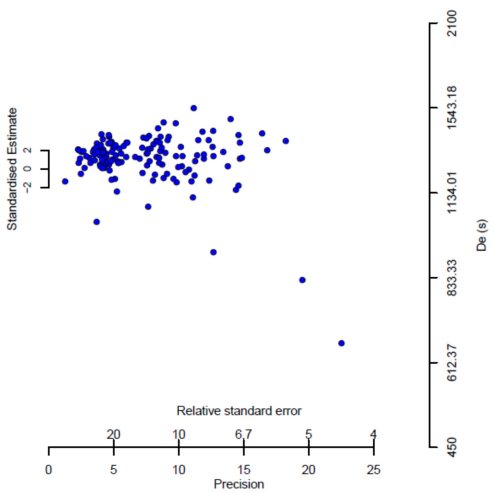

Figure 10. D_e distribution for 144 single grains from sample HF11 calculated using function `calSARED()` visualized using a pseudo radial plot.

The commands in lines 62–72 were used to calculate SGC D_e according to the method of Li et al. (2016). Objects `res_lsNORM$LMpars2[,1]` and `res_lsNORM$avg.error2` stand for the best-fit parameters and associated average deviation of the SGC established using LS-normalisation, respectively. Note that in order to calculate SGC D_e using the method of Li et al. (2016), the sensitivity-corrected natural signal and an additional sensitivity-corrected regenerative-dose signal need be specified (via argument `SAR.Cycle`). `SAR.Cycle=c("N","R2")` means that the second regenerative dose will be used to re-scale the natural signals for SGC D_e calculation. Figure 13 shows results of SGC D_e calculation for an aliquot of the fluvial sample.

```
62 res_gSGCED <- calSGCED(
63   res_analyseBINdata1,
64   SGCpars=res_lsNORM$LMpars2[,1],
65   model="gok", origin=FALSE,
66   avgDev=res_lsNORM$avg.error2,
67   method="gSGC", errMethod="sp",
68   SAR.Cycle=c("N","R2"),
69   Tn.above.3BG=TRUE,
70   TnBG.ratio.low=3,
71   rseTn.up=30, use.se=TRUE,
72   outpdf="gSGCED")
```

Finally, to test the reliability of SGC D_e determined above, we compared the SGC D_e values with those determined using the full SAR protocol. SAR D_e calculation using the data sets stored in object `res_analyseBINdata1` was implemented using the commands in lines 73–83. Here the fitting model and method used for D_e error assessment were chosen to be consistent with those used in SGC D_e calculation performed above. The commands in lines 84–87 used the **R** internal function `intersect()` to identify aliquots that succeed in both SAR and SGC D_e calculations.

```
73 res_SARED <- calSARED(
74   res_analyseBINdata1,
75   model="gok", origin=FALSE,
76   errMethod="sp",
77   Tn.above.3BG=TRUE,
78   TnBG.ratio.low=3,
79   rseTn.up=30,
80   rcy1.range=c(0.9,1.1),
81   rcp1.up=10, fom.up=10,
82   rcs.up=5, use.se=TRUE,
83   calED.method="Interpolation")
```

```
84 index <- intersect(intersect(
85   rownames(res_SARED$sarED),
86   rownames(res_SGCED$sgcED)),
87   rownames(res_gSGCED$sgcED))
```

The commands in lines 88–118 compare calculated D_e values between SAR and SGC using a scatter plot. The SAR D_e (lines 88–89) and SGC D_e calculated using the method of Li et al. (2016) (lines 90–91) were used as the x and y coordinates, respectively. To compare SAR D_e with SGC D_e calculated using the method of Roberts & Duller (2004), the user only needs to change `res_gSGCED` in lines 90–91 to `res_SGCED`. The commands in lines 103–106 and 107–110 add error bars to the x and y coordinates, respectively. The commands in lines 112–114 use the **R** internal function `cor()` to calculate the Pearson correlation coefficient between SAR and SGC D_e.

```
88 sarED <- res_SARED$sarED[index,1]
89 sarEDerr <-  res_SARED$sarED[index,2]
```

```
90 sgcED <- res_gSGCED$sgcED[index,1]
91 sgcEDerr <- res_gSGCED$sgcED[index,2]
```

```
92 min_xy <- min(sarED-sarEDerr,
93   sgcED-sgcEDerr)
94 max_xy <- max(sarED+sarEDerr,
95   sgcED+sgcEDerr)
```

```
96 plot(sarED, sgcED,
97   xlim=c(min_xy,max_xy),
98   ylim=c(min_xy,max_xy),
99   xlab="SAR De (s)",
100  ylab="SGC De (s)",
101  pch=21, bg="skyblue3",
102  col="skyblue3", cex=1.5)
```

```
103 arrows(x0=sarED-sarEDerr/2,
104   x1=sarED+sarEDerr/2,
105   y0=sgcED, y1=sgcED, code=3,
106   angle=90, length=0.05)
```

```
107 arrows(x0=sarED,
108   y0=sgcED-sgcEDerr/2,
109   x1=sarED, y1=sgcED+sgcEDerr/2, code=3,
110   angle=90, length=0.05)
```

```
111 abline(a=0, b=1, lty="dashed")
```

```
112 R2 <- round(
113   (cor(x=sarED, y=sgcED,
114   method="pearson"))^2, 3L)
```

```
115 legend("bottomright",
116   legend=c(paste("N=",
117   length(index)),
118   paste("R^2=", R2)), bty="n")
```

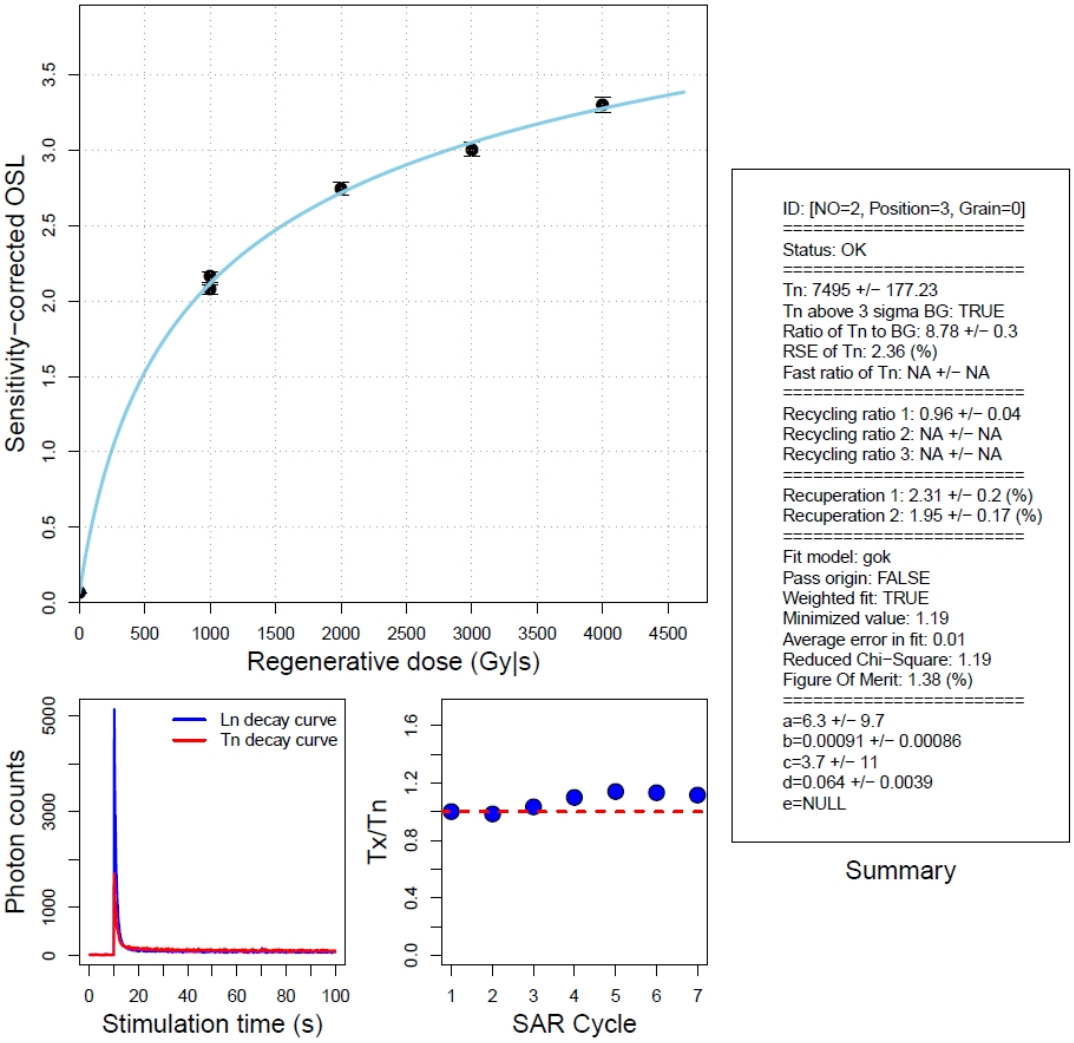

Figure 11. Results of growth curve selection produced using function `pickSARdata()` for one of the aliquots of a fluvial sample from Shanxi province in China. The upper plot shows result of growth curve fitting. The lower left plot shows the decay curves for the natural dose and its test dose. The lower right plot demonstrates the variation in the ratio of T_x to T_n for different SAR cycles. The right panel summarises the results of growth curve fitting. Note that the unit of dose is in irradiation time (second) rather than in Gy.

The commands in lines 119–127 visualize the distribution of ratios of SGC to SAR D_e using the pseudo radial plot. The standard errors of the ratios were calculated using command line 120–122. The commands in lines 123–127 use function `psRadialPlot()` from package '`numOSL`' to visualize the distribution of the ratios with a simplified (pseudo) radial plot. The central value was set equal to 1.0 (`dose=1.0`). The size of points can be modified using argument `psize`. Figure 14 shows comparisons between SAR D_e and SGC D_e calculated using two different methods.

```
119 Ratio <- sgcED/sarED

120 seRatio <- Ratio*
121   sqrt((sarEDerr/sarED)^2+
122   (sgcEDerr/sgcED)^2)

123 psRadialPlot(
124   cbind(Ratio,seRatio),
125   dose=1.0, zmin=0.7,
126   zmax=1.5, psize=1.5,
127   zlabel="Ratio of SGC to SAR De")
```

4. Discussion

A number of functions have been provided to flexibly import, select and analyse OSL data measured using a SAR procedure. The commonly used method for assessing the error estimate of the net OSL response is based on the assumption that the variance of photon counts follows a Poisson distribution (Galbraith, 2002). However, recent studies (Li, 2007; Adamiec et al., 2012) suggest that the variation in photon counts are dispersed more than would be expected from a Poisson distribution. The function `analyseBINdata()` estimates the standard error of net OSL signal using the newly derived formula outlined by Bluszcz et al. (2015) when count numbers do not follow a Poisson distribution. The function

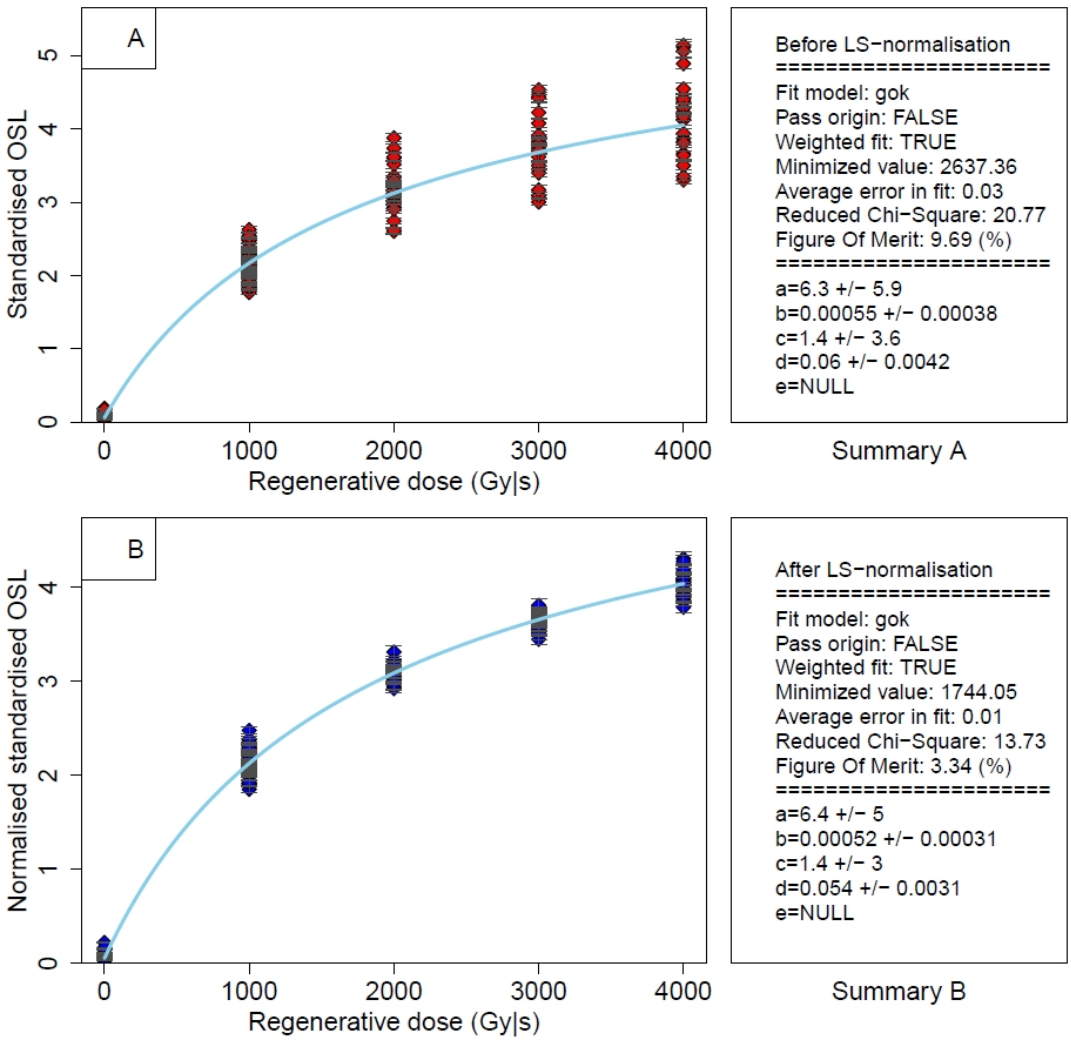

Figure 12. Results of LS-normalisation generated using function `lsNORM()`. The parameters (*a*, *b*, *c*, and *d*) shown in the right panel are obtained by fitting the data shown in the left panels using the GOK model. It should be noted that if the fitting is performed using a weighted procedure (i.e., `weight=TRUE`) then the "Minimized value" denotes the minimized chi-square value. For un-weighted fitting procedures (i.e., `weight=FALSE`), the "Minimized value" represents the minimized sum of squared residuals. The "Average error in fit" denotes the average deviation (*avgDev*) of the fitted growth curve data. Note that the unit of dose is in irradiation time (second) rather than in Gy.

was used to analyse single-grain data from sample HF11 (Li et al., 2016) and the results were compared to those analysed using *Analyst*. This comparison suggests that the sensitivity-corrected natural signal and associated standard error estimated using the two software packages are identical to each other when a Poisson distribution is assumed (Fig. 4A–B), but greater standard errors are obtained when photon counts do not follow a Poisson distribution (Fig. 4C).

Several strategies have been adopted to improve the efficiency, applicability, and practicability of the function `calSARED()` for SAR D_e analysis. Firstly, the core function has been programmed using the Fortran 90, instead of using pure **R** language, and wrapped by **R** using an interface. Compared to Fortran 90, pure **R** language has much less efficiency in the routine if a large number of SAR data sets are analysed (as shown in the worked example of Sec. 3.1). Secondly, the general applicability and robustness of the model used for growth curve fitting are critical for ensuring determination of a large number of D_e values in a batch model without the need for manual interference. Accordingly, besides the most commonly used models (i.e., the LINE, EXP, LEXP, and DEXP), the newly developed GOK model (Guralnik et al., 2015) has been included in our program. We tested the performance of this model using a large number of single-grain growth curve data from sample HF11 and other samples (data not shown here). Our results demonstrate the general applicability and robustness of the GOK model in growth curve fitting (as shown in Fig. 5). Moreover, setting argument `trial=TRUE` ensures that the growth curve will be fitted using other models if the specified model fails. This further increases the flexibility and adaptability of the function in growth curve fitting. Finally, we have integrated the commonly used rejection criteria for selecting and rejecting SAR D_e estimates into the function `calSARED()`. These cri-

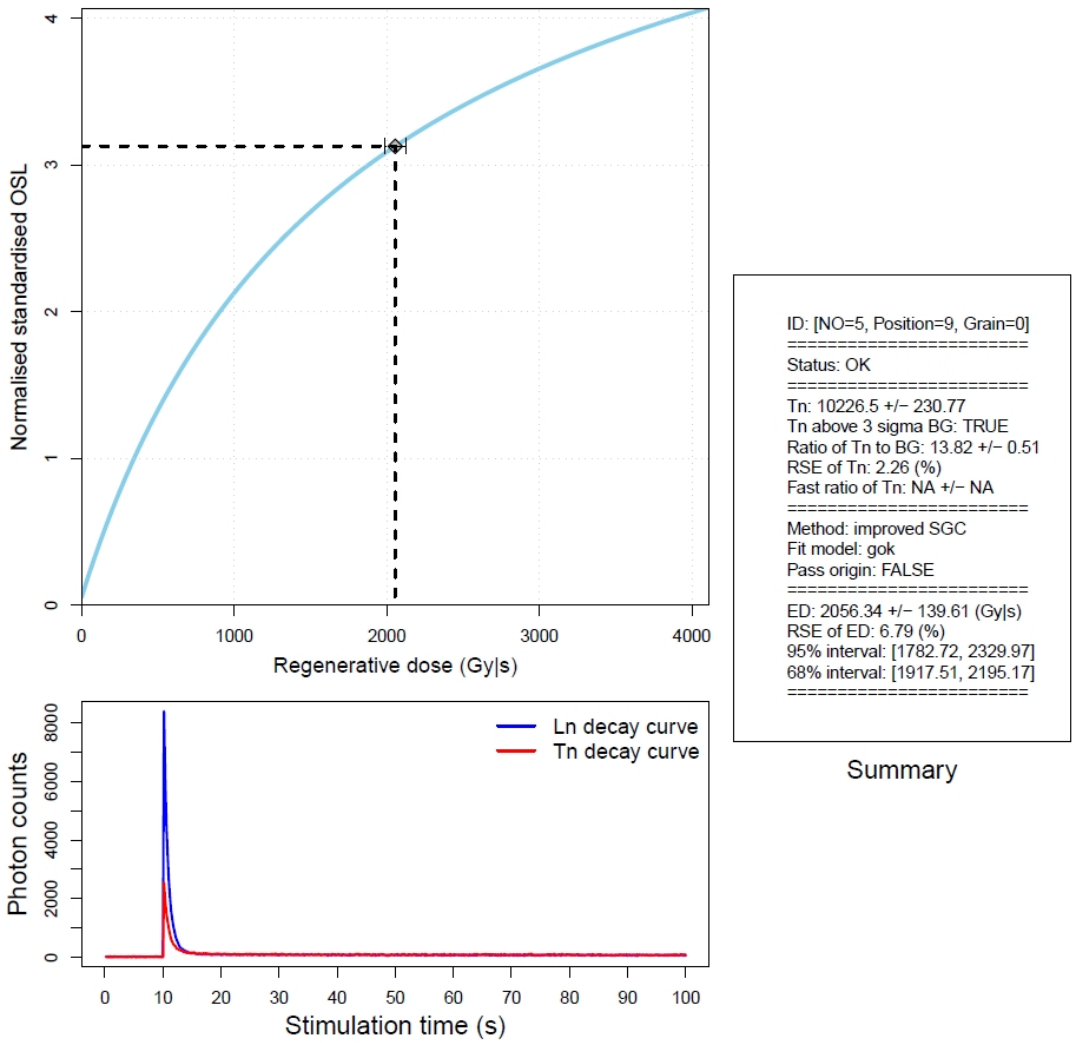

Figure 13. Results of SGC D_e calculation produced using function `calSGCED()` for one of the aliquots of a fluvial sample from Shanxi province in China. The upper plot shows result of SGC D_e calculation. The blue line denotes the SGC established using LS-normalisation. The lower plot shows the decay curves for the natural dose and its test dose. The right panel summarises the results of D_e calculation. The 68% (one sigma) and 95% (two sigma) confidence intervals of D_e were determined by normal approximation (not Monte Carlo simulation) as the simple transformation method is applied here for D_e error assessment. Note that the unit of dose is in irradiation time (second) rather than in Gy.

teria are applied in a manner that save calculation resources as much as possible. For this purpose, signal-related criteria are applied first, then the growth-curve-related criteria, and the D_e-related criteria are considered last. We compared SAR D_e and associated standard errors obtained from the function `calSARED()` with those estimated from *Analyst* (as shown in Fig. 7). The results between two software packages are indistinguishable.

Two criteria (FOM and RCS) are adopted to select reliable growth curves for SGC establishment. Generally, the FOM is useful in selecting "absolutely perfect" growth curves by ignoring their standard errors, while RCS also takes the standard errors into account. Note that the upper limits on FOM and RCS used to extract "acceptable" growth curves may be sample dependent, which needs to be further investigated and is beyond the scope of this study.

The performance of the LS-normalisation procedure implemented using the function `lsNORM()` was tested using randomly simulated growth curve data (as shown in Fig. 8). The results suggest that the LS-normalisation procedure is a generally reliable method for reducing variation in growth curves between aliquots (grains) measured from the same or different samples. However, we would like to emphasise here that the SGC method should only be applied on the basis of a careful validation, i.e., by comparing SAR and SGC D_e estimates using a large number of measured SAR data sets. It is necessary to first test whether reliable D_e estimates can be obtained using a full SAR procedure, and assess the effect and importance of each of the rejection criteria used to select SAR D_e; the latter is especially important because the SGC approach involves only the measurements of natural-dose and an additional regenerative-dose cycles, so

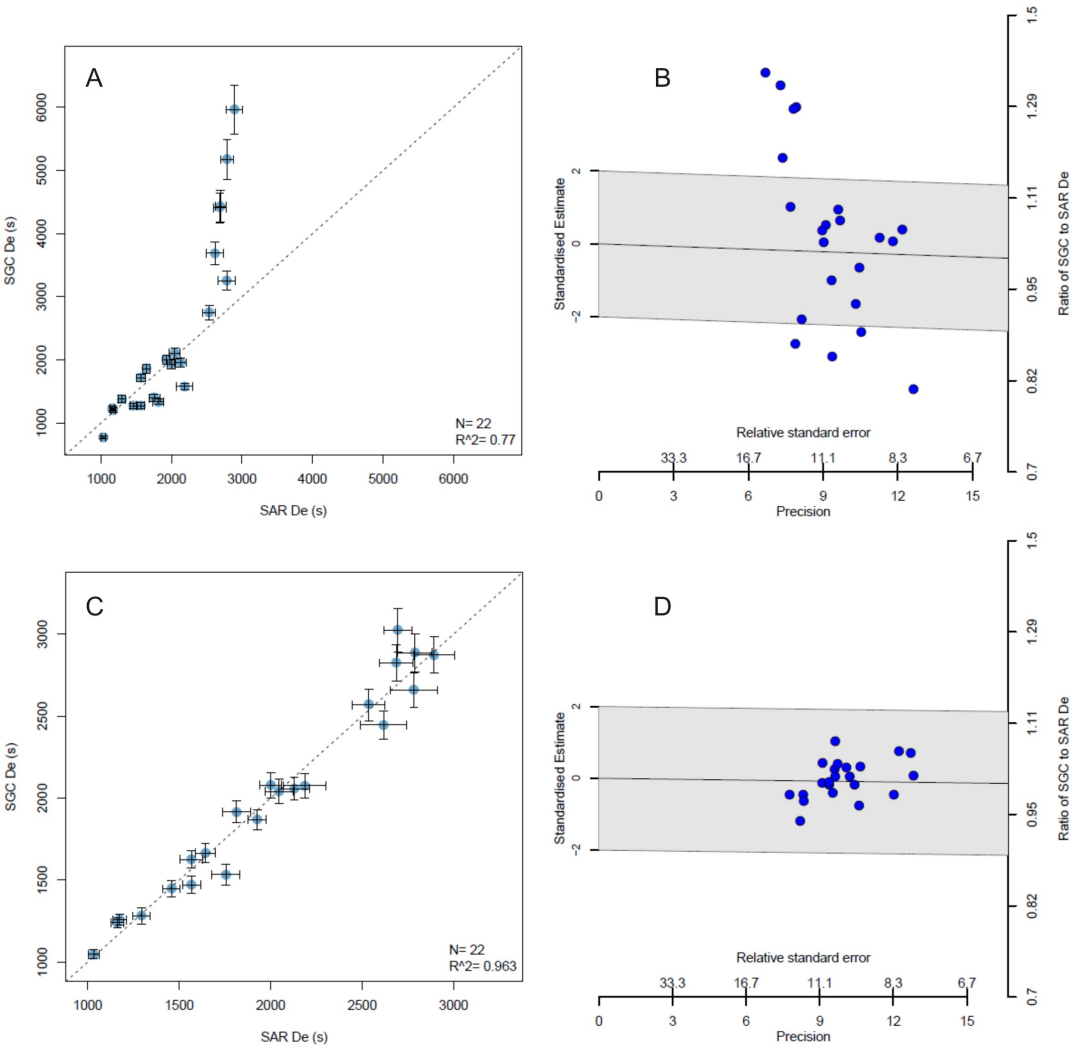

Figure 14. Comparison between SAR and SGC D_e estimates. (A) and (C) plot SAR D_e against SGC D_e determined using the methods of Roberts & Duller (2004) and Li et al. (2016), respectively. (B) and (D) show distributions of ratios of SGC D_e determined using the methods of Roberts & Duller (2004) and Li et al. (2016) to SAR D_e, respectively. The grey bands in (B) and (D) show the 2 sigma range around the central value at 1.

application of growth-curve-related rejection criteria (such as recuperation, recycling ratio, FOM, and RCS) is not possible. Consequently, the user may incorporate some poorly-behaved grains (e.g., Duller et al., 2000; Jacobs et al., 2003, 2006; Duller, 2008) into the final calculation, which may not only induce additional uncertainty in the final results but also may produce erroneous results.

Batch analysis of SAR and SGC data offers benefits for standardisation of analyses and elimination of user error, and, therefore, can substantially reduce the amount of data-handling time. At the same time, however, we would emphasis and maintain that manual data analysis also has its own advantages. We would like to suggest that one should conduct manual data analysis at least for some of their samples or some of the measured grains, particularly for understanding potentially problematic OSL behaviours, better characterisation of variable OSL properties between samples, and for identifying behavioural trends that might go unnoticed when using automated procedures. In reality, the optimum approach for SAR analysis of a large number of data sets undoubtedly lies in combining both practices together, particularly when working on previously unstudied samples: i.e., undertaking batch analysis for implementation of quality assurance criteria and for deriving accepted D_e populations, and then manually cross-checking the OSL properties of the rejected and accepted grain populations to ensure that sample-specific luminescence properties are fully understood by the user.

5. Conclusions

We present several general **R** functions to flexibly analyse SAR data and determine SAR and SGC D_e in a batch model under the framework of the `numOSL` package. The intended use of these functions is to enable the user to rapidly and flexibly perform D_e analysis for a large number of SAR

data sets. We have provided practical workflows, including data import (selection), signal analysis, SAR D_e determination, application of rejection criteria, growth curve selection, LS-normalisation, and SGC D_e calculation, using simple **R** code templates. We demonstrate that a combination of the small number of **R** functions can be used to perform SAR and SGC D_e analysis in a flexible and efficient manner. These functions are totally self-contained and do not depend on any external **R** packages. Users are encouraged to combine our program with other software packages (e.g., *Analyst*, **R** package `'Luminescence'`, etc.) for their specific SAR (SGC) application requirements.

Acknowledgments

Zenobia Jacobs is thanked for providing the example data from sample HF11. Valuable and constructive comments were provided by Lee Arnold. BL was supported by an Australian Research Council Future Fellowship grant (FT140100384). JP was supported by the National Natural Science Foundation of China (41701004).

References

Adamiec, G., Heer, A. J., and Bluszcz, A. *Statistics of count numbers from a photomultiplier tube and its implications for error estimation*. Radiation Measurements, 47(9): 746–751, 2012.

Armitage, S. J., Jasim, S. A., Marks, A. E., Parker, A. G., Usik, V. I., and Uerpmann, H. P. *The Southern Route "Out of Africa": Evidence for an Early Expansion of Modern Humans into Arabia*. Science, 331(6016): 453–456, 2011.

Arnold, L. J., Demuro, M., Navazo, M., Benito-Calvo, A., and Pérez-González, A. *OSL dating of the Middle Palaeolithic Hotel California site, Sierra de Atapuerca, north-central Spain*. Boreas, 42(2): 285–305, 2012.

Bailey, R. M. *Towards a general kinetic model for optically and thermally stimulated luminescence of quartz*. Radiation Measurements, 33(1): 17–45, 2001.

Balian, H. G. and Eddy, N. W. *Figure-of-merit (FOM), an improved criterion over the normalized chi-squared test for assessing goodness-of-fit of gamma-ray spectral peaks*. Nuclear Instruments and Methods, 145(2): 389–395, 1977.

Ballarini, M., Wallinga, J., Wintle, A. G., and Bos, A. J. J. *Analysis of equivalent-dose distributions for single grains of quartz from modern deposits*. Quaternary Geochronology, 2(1-4): 77–82, 2007.

Bevington, P. R. and Robinson, D. K. *Data Reduction and Error Analysis for the Physical Sciences*. McGraw-Hill Education, 2002. pp194–195.

Bluszcz, A., Adamiec, G., and Heer, A. J. *Estimation of equivalent dose and its uncertainty in the OSL SAR protocol when count numbers do not follow a Poisson distribution*. Radiation Measurements, 81: 46–54, 2015.

Bos, A. J. J., Piters, T. M., Gómez-Ros, J. M., and Delgado, A. *An Intercomparison of Glow Curve Analysis Computer Programs: II. Measured Glow Curves*. Radiation Protection Dosimetry, 51(4): 257–264, 1994.

Burbidge, C. I., Duller, G. A. T., and Roberts, H. M. *D_e determination for young samples using the standardised OSL response of coarse-grain quartz*. Radiation Measurements, 41(3): 278–288, 2006.

Douka, K., Jacobs, Z., Lane, C., Grün, R., Farr, L., Hunt, C., Inglis, R. H., Reynolds, T., Albert, P., Aubert, M., Cullen, V., Hill, E., Kinsley, L., Roberts, R. G., Tomlinson, E. L., Wulf, S., and Barker, G. *The chronostratigraphy of the Haua Fteah cave (Cyrenaica, northeast Libya)*. Journal of Human Evolution, 66: 39–63, 2014.

Duller, G. A. T. *Distinguishing quartz and feldspar in single grain luminescence measurements*. Radiation Measurements, 37(2): 161–165, 2003.

Duller, G. A. T. *Assessing the error on equivalent dose estimates derived from single aliquot regenerative dose measurements*. Ancient TL, 25(1): 15–24, 2007.

Duller, G. A. T. *Single-grain optical dating of Quaternary sediments: why aliquot size matters in luminescence dating*. Boreas, 37(4): 589–612, 2008.

Duller, G. A. T. *Improving the accuracy and precision of equivalent doses determined using the optically stimulated luminescence signal from single grains of quartz*. Radiation Measurements, 47(9): 770–777, 2012.

Duller, G. A. T. *The Analyst software package for luminescence data: overview and recent improvements* . Ancient TL, 33(1): 35–42, 2015.

Duller, G. A. T., Bøtter-Jensen, L., and Murray, A. S. *Optical dating of single sand-sized grains of quartz: sources of variability*. Radiation Measurements, 32(5-6): 453–457, 2000.

Durcan, J. A. and Duller, G. A. T. *The fast ratio: A rapid measure for testing the dominance of the fast component in the initial OSL signal from quartz*. Radiation Measurements, 46(10): 1065–1072, 2011.

Feathers, J. K. *Single-grain OSL dating of sediments from the Southern High Plains, USA*. Quaternary Science Reviews, 22(10-13): 1035–1042, 2003.

Fu, X., Li, B., and Li, S. H. *Testing a multi-step post-IR IRSL dating method using polymineral fine grains from Chinese loess*. Quaternary Geochronology, 10: 8–15, 2012.

Fu, X., Cohen, T. J., and Arnold, L. J. *Extending the record of lacustrine phases beyond the last interglacial for Lake Eyre in central Australia using luminescence dating*. Quaternary Science Reviews, 162: 88–110, 2017.

Galbraith, R. F. *Graphical Display of Estimates Having Differing Standard Errors*. Technometrics, 30(3): 271–281, 1988.

Galbraith, R. F. *A note on the variance of a background-corrected OSL count*. Ancient TL, 20(2): 49–51, 2002.

Galbraith, R. F. and Roberts, R. G. *Statistical aspects of equivalent dose and error calculation and display in OSL dating: An overview and some recommendations*. Quaternary Geochronology, 11: 1–27, 2012.

Galbraith, R. F., Roberts, R. G., Laslett, G. M., Yoshida, H., and Olley, J. M. *Optical dating of single and multiple grains of Quartz from Jinmium Rock Shelter, Northern Australia: Part I, Experimental design and statistical models*. Archaeometry, 41(2): 339–364, 1999.

Guo, Y. J., Li, B., Zhang, J. F., Yuan, B. Y., Xie, F., and Roberts, R. G. *Luminescence ages for three 'Middle Palaeolithic' sites in the Nihewan Basin, northern China, and their archaeological and palaeoenvironmental implications*. Quaternary Research, 85(3): 456–470, 2016.

Guralnik, B., Li, B., Jain, M., Chen, R., Paris, R. B., Murray, A. S., Li, S. H., Pagonis, V., Valla, P. G., and Herman, F. *Radiation-induced growth and isothermal decay of infrared-stimulated luminescence from feldspar*. Radiation Measurements, 81: 224–231, 2015.

Horowitz, Y. S. and Yossian, D. *Computerised Glow Curve Deconvolution: Application to Thermoluminescence Dosimetry*. Radiation Protection Dosimetry, 60(1): 3–111, 1995.

Hu, G., Yi, C. L., Zhang, J. F., Liu, J. H., Jiang, T., and Li, S. H. *Late Quaternary glacial advances in the eastern Qilianshan, north-eastern Tibet, as inferred from luminescence dating of fluvioglacial sediments*. Journal of Quaternary Science, 31(6): 587–597, 2016.

Jacobs, Z., Duller, G. A. T., and Wintle, A. G. *Optical dating of dune sand from Blombos Cave, South Africa: II—single grain data*. Journal of Human Evolution, 44(5): 613–625, 2003.

Jacobs, Z., Duller, G. A. T., and Wintle, A. G. *IInterpretation of single grain D_e distributions and calculation of D_e*. Radiation Measurements, 41(3): 264–277, 2006.

Jacobs, Z., Li, B., Jankowski, N., and Soressi, M. *Testing of a single grain OSL chronology across the Middle to Upper Palaeolithic transition at Les Cates (France)*. Journal of Archaeological Science, 54: 110–122, 2015.

Jacobs, Z., Li, B., Farr, L., Hill, E., Hunt, C., Jones, S., Rabett, R., Reynolds, T., Roberts, R. G., Simpson, D., and Barker, G. *The chronostratigraphy of the Haua Fteah cave (Cyrenaica, northeast Libya) - Optical dating of early human occupation during Marine Isotope Stages 4, 5 and 6*. Journal of Human Evolution, 105: 69–88, 2017.

Kreutzer, S., Schmidt, C., Fuchs, M., Dietze, M., Fischer, M., and Fuchs, M. *Introducing an R package for luminescence dating analysis* . Ancient TL, 30(1): 1–8, 2012.

Lai, Z. P. *Testing the use of an OSL standardised growth curve (SGC) for D_e determination on quartz from the Chinese Loess Plateau*. Radiation Measurements, 41(1): 9–16, 2006.

Li, B. *A note on estimating the error when subtracting background counts from weak OSL signals*. Ancient TL, 25(1): 9–14, 2007.

Li, B., Jacobs, Z., Roberts, R. G., and Li, S. H. *Extending the age limit of luminescence dating using the dose-dependent sensitivity of MET-pIRIR signals from K-feldspar*. Quaternary Geochronology, 17: 55–67, 2013.

Li, B., Roberts, R. G., Jacobs, Z., and Li, S. H. *A single-aliquot luminescence dating procedure for K-feldspar based on the dose-dependent MET-pIRIR signal sensitivity*. Quaternary Geochronology, 20: 51–64, 2014.

Li, B., Roberts, R. G., Jacobs, Z., and Li, S. H. *Potential of establishing a 'global standardised growth curve' (gSGC) for optical dating of quartz from sediments*. Quaternary Geochronology, 27: 94–104, 2015a.

Li, B., Roberts, R. G., Jacobs, Z., Li, S. H., and Guo, Y. J. *Construction of a 'global standardised growth curve' (gSGC) for infrared stimulated luminescence dating of K-feldspar*. Quaternary Geochronology, 27: 119–130, 2015b.

Li, B., Jacobs, Z., and Roberts, R. G. *Investigation of the applicability of standardised growth curves for OSL dating of quartz from Haua Fteah cave, Libya*. Quaternary Geochronology, 35: 1–15, 2016.

Long, H., Lai, Z. P., Fan, Q. S., Sun, Y. J., and Liu, X. J. *Applicability of a quartz OSL standardised growth curve for De determination up to 400Gy for lacustrine sediments from the Qaidam Basin of the Qinghai-Tibetan Plateau*. Quaternary Geochronology, 5(2-3): 212–217, 2010.

Madsen, A. T., Duller, G. A. T., Donnelly, J. P., Roberts, H. M., and Wintle, A. G. *A chronology of hurricane landfalls at Little Sippewissett Marsh, Massachusetts, USA, using optical dating*. Geomorphology, 109(1-2): 36–45, 2009.

Moré, J. J. *The Levenberg-Marquardt algorithm: Implementation and theory*. In *Numerical Analysis*, pp. 105–116. Springer, Berlin, Heidelberg, 1978.

Murray, A. S. and Olley, J. M. *Precision and Accuracy in the optically stimulated luminescence dating of sedimentary quartz: a status review*. Geochronometria, 21: 1–16, 2002.

Murray, A. S. and Wintle, A. G. *Luminescence dating of quartz using an improved single-aliquot regenerative-dose protocol*. Radiation Measurements, 32(1): 57–73, 2000.

Pagonis, V. and Kitis, G. *On the Possibility of using Commercial Software Packages for Thermoluminescence Glow Curve Deconvolution Analysis*. Radiation Protection Dosimetry, 101(1–4): 93–98, 2002.

Peng, J. and Pagonis, V. *Simulating comprehensive kinetic models for quartz luminescence using the R program KMS*. Radiation Measurements, 86: 63–70, 2016.

Peng, J., Dong, Z., Han, F. Q., Long, H., and Liu, X. J. *R package numOSL: numeric routines for optically stimulated luminescence dating*. Ancient TL, 31(2): 41–48, 2013.

Peng, J., Pagonis, V., and Li, B. *On the intrinsic accuracy and precision of the standardised growth curve (SGC) and global-SGC (gSGC) methods for equivalent dose determination: A simulation study*. Radiation Measurements, 94: 53–64, 2016.

Roberts, H. M. and Duller, G. A. T. *Standardised growth curves for optical dating of sediment using multiple-grain aliquots*. Radiation Measurements, 38(2): 241–252, 2004.

Roberts, R. G., Jacobs, Z., Li, B., Jankowski, N. R., Cunningham, A. C., and Rosenfeld, A. B. *Optical dating in archaeology: thirty years in retrospect and grand challenges for the future*. Journal of Archaeological Science, 56: 41–60, 2015.

Shen, Z. and Mauz, B. *Estimating the equivalent dose of late Pleistocene fine silt quartz from the Lower Mississippi Valley using a standardized OSL growth curve*. Radiation Measurements, 46(8): 649–654, 2011.

Stevens, T., Armitage, S. J., Lu, H., and Thomas, D. S. G. *Examining the potential of high sampling resolution OSL dating of Chinese loess*. Quaternary Geochronology, 2(1–4): 15–22, 2007.

Telfer, M. W., Bateman, M. D., Carr, A. S., and Chase, B. M. *Testing the applicability of a standardized growth curve (SGC) for quartz OSL dating: Kalahari dunes, South African coastal dunes and Florida dune cordons*. Quaternary Geochronology, 3(1–2): 137–142, 2008.

Wintle, A. G. and Murray, A. S. *A review of quartz optically stimulated luminescence characteristics and their relevance in single-aliquot regeneration dating protocols*. Radiation Measurements, 41(4): 369–391, 2006.

Xie, Y. H. *Dynamic Documents with R and knitr*. Chapman & Hall/CRC Press, 2015. pp17–18.

Yang, L. H., Lai, Z. P., Long, H., and Zhang, J. R. *Construction of a quartz OSL standardised growth curve (SGC) for aeolian samples from the Horqin dunefield in northeastern China*. Geochronometria, 38(4): 391–396, 2011.

Reviewer

Lee Arnold